JACS
JOURNAL OF THE AMERICAN CHEMICAL SOCIETY
Article
pubs.acs.org/JACS

Understanding Carbon Dioxide Adsorption on Univalent Cation Forms of the Flexible Zeolite Rho at Conditions Relevant to Carbon Capture from Flue Gases

Magdalena M. Lozinska,[†] Enzo Mangano,[‡] John P. S. Mowat,[†] Ashley M. Shepherd,[§] Russell F. Howe,[§] Stephen P. Thompson,[∥] Julia E. Parker,[∥] Stefano Brandani,[‡] and Paul A. Wright*[,†]

[†]EaStCHEM School of Chemistry, University of St. Andrews, Purdie Building, North Haugh, St Andrews, Fife KY16 9ST, Scotland
[‡]Institute for Materials and Processes, University of Edinburgh, King's Buildings, Mayfield Rd, Edinburgh EH9 3JL, Scotland
[§]Department of Chemistry, University of Aberdeen, Meston Building, King's College, Aberdeen AB24 3UE, Scotland
[∥]Diamond Light Source Ltd., Harwell Science and Innovation Campus, Didcot, Oxfordshire OX11 0DE, U.K.

Supporting Information

ABSTRACT: A series of univalent cation forms of zeolite Rho ($M_{9.8}Al_{9.8}Si_{38.2}O_{96}$, M = H, Li, Na, K, NH_4, Cs) and ultrastabilized zeolite Rho (US-Rho) have been prepared. Their CO_2 adsorption behavior has been measured at 298 K and up to 1 bar and related to the structures of the dehydrated forms determined by Rietveld refinement and, for H-Rho and US-Rho, by solid state NMR. Additionally, CO_2 adsorption properties of the H-form of the silicoalumino-phosphate with the RHO topology and univalent cation forms of the zeolite ZK-5 were measured for comparison. The highest uptakes at 0.1 bar, 298 K for both Rho and ZK-5 were obtained on the Li-forms (Li-Rho, 3.4 mmol g^{-1}; Li-ZK-5, 4.7 mmol g^{-1}). H- and US-Rho had relatively low uptakes under these conditions: extra-framework Al species do not interact strongly with CO_2. Forms of zeolite Rho in which cations occupy window sites between α-cages show hysteresis in their CO_2 isotherms, the magnitude of which (Na^+,NH_4^+ < K^+ < Cs^+) correlates with the tendency for cations to occupy double eight-membered ring sites rather than single eight-membered ring sites. Hysteresis is not observed for zeolites where cations do not occupy the intercage windows. *In situ* synchrotron X-ray diffraction of the CO_2 adsorption on Na-Rho at 298 K identifies the adsorption sites. The framework structure of Na-Rho "breathes" as CO_2 is adsorbed and desorbed and its desorption kinetics from Na-Rho at 308 K have been quantified by the Zero Length Column chromatographic technique. Na-Rho shows much higher CO_2/C_2H_6 selectivity than Na-ZK-5, as determined by single component adsorption, indicating that whereas CO_2 can diffuse readily through windows containing Na^+ cations, ethane cannot.

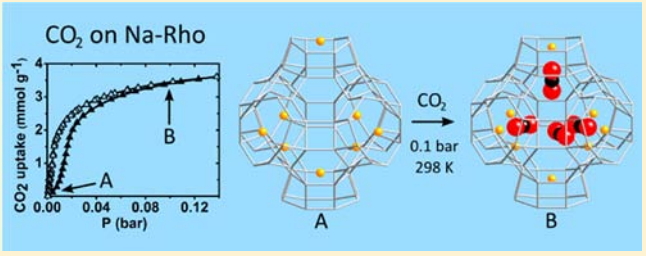

1. INTRODUCTION

Cationic zeolites with relatively high extra-framework cation contents are effective CO_2 adsorbents that can adsorb significant amounts of this greenhouse gas even at the low partial pressures of CO_2 (*ca.* 0.1 bar) and ambient temperatures relevant to carbon capture from flue gases.[1−7] Zeolites A, X, and Y, for example, which have relatively low Si/Al ratios and high extra framework cation contents adsorb CO_2 strongly at ambient temperature.[1−3] In each of these zeolites, however, much of the open space is inaccessible to CO_2 because the sodalite cages that are part of these structures cannot admit CO_2 (because it cannot pass through their six-membered ring (6MR) openings). Another approach is to use zeolites that have a larger fraction of their pore volume accessible but still have relatively small cages that facilitate strong interactions with adsorbed molecules, even at the highest levels of pore filling. The zeolites chabazite[4−7] and Rho[8] are attractive in this regard. In chabazitic zeotypes, for example, pore volumes of 0.33 cm^3 g^{-1} are available if no pore space is taken up by extra-framework cations, whereas in Rho, where all pore space is available, this value (see later) is 0.36 cm^3 g^{-1}.

Ridha et al. report the adsorption of CO_2 on Li-, Na-, and K-chabazite,[4−6] indicating that uptakes of between 4 and 5 mmol g^{-1} were obtained at 303 K and 0.1 bar, with the highest values obtained for Li-chabazite due to the high electrostatic interactions on the small Li^+ cation. The presence of the larger K^+ cation in the pores imparts the advantage of increasing the selectivity over N_2, which is both larger and interacts more weakly than CO_2 and so is less readily taken up. Hudson et al. report CO_2 adsorption on Cu-SSZ-13 (a high Si/Al chabazite) to be selective, although with lower uptake, and attribute the selectivity to the favorable interaction with the framework rather than with the extra-framework Cu^{2+} cations.[7] Very

Received: July 19, 2012
Published: September 26, 2012

   dx.doi.org/10.1021/ja3070864 | J. Am. Chem. Soc. 2012, 134, 17628−17642

recently, work on zeolite Na,Cs-Rho by Palomino et al.[9] showed very high CO_2/CH_4 selectivity at <1 bar and also non-type I adsorption behavior for CO_2 above *ca.* 1 bar that results from the structural flexibility of the Rho structure. *In situ* X-ray diffraction showed that at pressures of around 1 bar the framework structure undergoes the transformation from *I*-43*m* to *Im*-3*m* that is well characterized for Rho, in which both the pore volume and the window size increases (Figure 1).[10] Also,

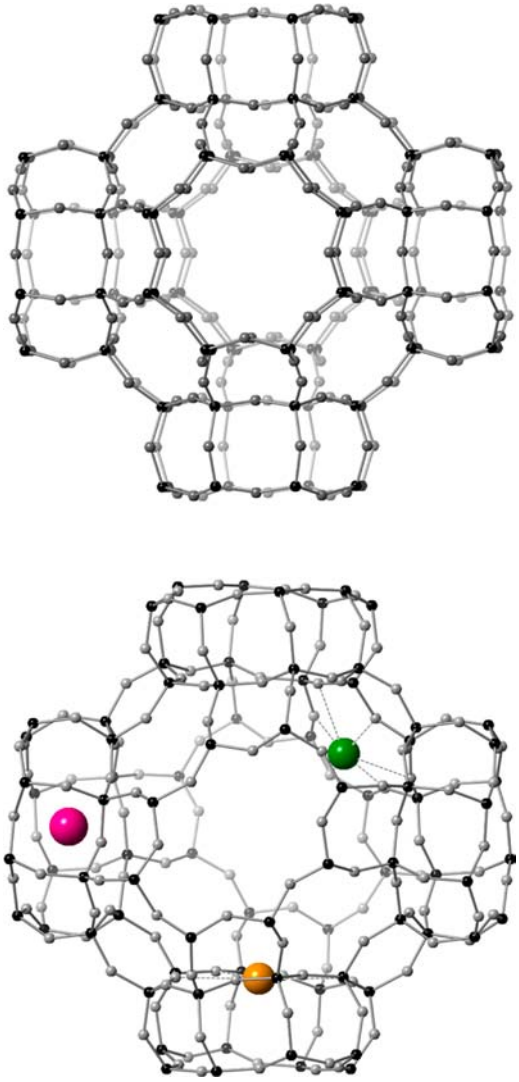

Figure 1. (Top) Framework structure of zeolite Rho in *Im*-3*m* symmetry, showing an α-cage surrounded by six double eight-membered ring (D8R) units that act as windows. (Bottom) Structure of zeolite Rho in *I*-43*m* symmetry, showing position of extra-framework cations in sites of type I, D8R, red sphere; type II, single eight-membered ring, S8R, orange sphere; and type III, single six-membered ring, S6R, green sphere.

recent publication of CO_2 isotherms on a range of different cation forms of zeolite Rho show strongly compositional adsorption effects and also strong hysteresis and non-type I behavior.[11] Only a very general explanation was suggested for this complex behavior, which is expected to result in part from the extra-framework cation distribution and strong cation-dependent structural flexibility of the Rho structure.[12−15]

We report here measurements of CO_2 adsorption on zeolite Rho samples fully exchanged with a range of univalent cations (Li^+, Na^+, K^+, Cs^+, NH_4^+, H^+) prepared by exhaustive cation exchange. The presence of univalent cations (other than protons) is observed to prevent the uptake of N_2 at 77 K but allow CO_2 uptake at 298 K, and CO_2 adsorption isotherms reveal a range of behavior, including strong deviation from Type I adsorption and hysteresis. Additional insight is available from measurements of reversible CO_2 uptake made using the Zero Length Column (ZLC) method[16−19] on fully and partially cation-exchanged samples. These data on zeolite Rho are compared with similar measurements performed on a zeolite ZK-5[20,21] of framework composition similar to that of the Rho studied here: ZK-5 is a structure that does not show flexibility upon dehydration and acts as a good example of a rigid, small pore structure with permanent porosity to N_2 and CO_2. In a first step, the adsorption behavior of all Rho and ZK-5 materials has been discussed by reference to the crystal structures of the dehydrated forms.

The CO_2 adsorption on zeolite Rho is found to be a complex function of cation type and loading. According to these measurements, and also because sodium is inexpensive, Na-Rho possesses the most potential as an adsorbent for the selective uptake of CO_2 at reasonable rates and with accessible uptake capacity at low partial pressures and ambient temperatures. Consequently, the mechanism of CO_2 adsorption and desorption on Na-Rho under conditions relevant to carbon capture from flue gases was studied in greater depth by a combination of *in situ* powder synchrotron XRD and IR spectroscopy. These reveal the response of the framework structure to CO_2 uptake and desorption and locate and quantify the adsorption sites for CO_2. The strongest CO_2 adsorption sites involve coordination of the molecules with extra-framework Na^+ cation sites, in a way similar to that proposed previously from modeling studies for adsorption of zeolites Na-Y,[2] Na-ferrierite,[22] and Na-A.[23] In addition to providing sites for strong adsorption via electrostatic interactions, the Na^+ cations occupy sites in single eight-membered ring (S8R) sites in windows between the α-cages and must move away from these window sites to enable adsorption to occur. The CO_2 diffusivity on Na-Rho at "zero coverage" has been measured directly using the versatile ZLC method.[16−19]

2. EXPERIMENTAL SECTION

Zeolite Na,Cs-Rho was prepared in the presence of 18-crown-6 according to published procedures.[24,25] The silicoaluminophosphate (SAPO) form of Rho[26] and the zeolite K-ZK-5[21] were also synthesized according to published methods. EDX analysis on these and all other samples was performed in a JEOL JSM 5600 SEM, with an Oxford INCA Energy 200 EDX analyzer. In addition, the morphology of zeolite Rho crystals was measured by field emission scanning electron microscopy (FEG-SEM) on a Jeol JSM-6700F electron microscope. Solid-state ^{27}Al and ^{29}Si MASNMR were performed on selected samples using a Varian VNMRS spectrometer operating at 79.44 MHz for ^{29}Si and 104.20 MHz for ^{27}Al. Deconvolution of the ^{29}Si MASNMR of the as-prepared Na,Cs-Rho, in which all aluminum occupies tetrahedral sites, was used to determine the framework Si/Al ratio of zeolite Rho and used to calibrate the Si/Al ratios determined via EDX.

The as-prepared Na,Cs-crown ether form of zeolite Rho was calcined at 823 K in oxygen for 12 h to remove all organic molecules. The resulting Na,Cs-Rho was fully exchanged to the ammonium form with 3 M ammonium chloride solution at 333 K, eight times for 5 h, until no cesium or sodium could be observed by EDX analysis. By contrast, most reported structural work on cationic forms of Rho[14] (often performed on larger multigram batches for neutron diffraction studies[14]) possessed significant levels of Cs^+ cations, which influence

dx.doi.org/10.1021/ja3070864 | J. Am. Chem. Soc. 2012, 134, 17628−17642

the structural behavior upon dehydration and CO_2 adsorption. Subsequently the ammonium form was converted to sodium, potassium, and cesium forms by additional repeated extended cation exchange treatments at 353 K using 10 wt % metal nitrate solutions, according to published procedures.[15,27] Finally, the lithium form of zeolite Rho was prepared by lithium exchange of the sodium form until no sodium could be observed by EDX. The lithium content was confirmed by subsequent repeated ion exchange with ammonium and measurement by atomic absorption of the lithium content of the resulting solutions. Any residual trace ammonium was converted to H^+ prior to all subsequent adsorption, structural, and spectroscopic measurements by heating at 623 K prior to analysis.

It was also possible to prepare mixed Li/NH_4 and Na/NH_4 zeolite Rho solids (general formula $(M^+)_{x-y}(NH_4^+)_yAl_xSi_{1-x}O_2$ via careful removal of cations by subsequent controlled ion exchange at 333 K for 30 min. Weighed portions (0.2 g) of Na-Rho and Li-Rho zeolites were stirred with 10 mL of ammonium chloride solution, with concentrations in the range of 0.01−3 M NH_4Cl. The amount of sodium remaining in the Na,NH_4-zeolites was determined by EDX. To determine the lithium content of the Li,NH_4-zeolites, the amount of Li^+ ions lost to the solution during ion exchange was measured by atomic absorption spectroscopy.

Thermogravimetry of all pure univalent cation forms of Rho was performed using a Netzsch TG 209 instrument with a heating rate of 5 K min^{-1} up to 973 K in flowing air, in order to determine the temperature at which water (or ammonia in the case of NH_4-Rho) was evolved (see Supporting Information). The protonic form of zeolite Rho and mixed cation/H^+-forms were prepared via deammoniation of the parent NH_4- or mixed NH_4/M-forms by heating under shallow bed conditions in dry flowing nitrogen at 823 K for 12 h, conditions known from literature data[10,28] and also our own TGA analysis to result in complete NH_3 removal. In addition, a sample of NH_4-Rho was "steamed" by heating under a high partial pressure of H_2O, to prepare "ultrastabilized" Rho, US-Rho.[14,29,30] In these experiments, a bed of pelletized NH_4-Rho was steamed in water vapor using water flow rates of 2.0 mL h^{-1} in flowing nitrogen at 743, 773 ,and 823 K for 8 h. To follow the effects of the deammoniation and steaming, ^{29}Si and ^{27}Al MASNMR were performed as described above, and for the sample steamed at 743 K, a two-dimensional ^{27}Al MQMAS spectra was obtained using a pulse sequence consisting of two pulses (of duration 2.8 and 1.0 μs at an RF field equivalent to 105 kHz) and a z-filter (at an RF field equivalent to 15 kHz). A total of 4000 repetitions were acquired for each of 32 increments in t_1. The recycle delay was 0.2 s, and the spinning rate was 12 kHz. Spectral referencing is with respect to external 1 M aqueous $AlCl_3$. The spectrum is plotted after shearing, and the indirectly detected, "isotropic", axis is scaled by a factor of 12/31. The protonic form of SAPO Rho was prepared by calcination in O_2 at 823 K for 12 h, conditions known to remove the organic template.

For comparison, sodium and lithium forms of ZK-5 were obtained by repeated cation exchange of the as-prepared potassium form at 353 K (8 exchanges for 4 h, using 1 M chloride solutions). In this case small amounts of potassium were observed to remain by EDX, giving unit cell compositions of $Na_{16.6}K_2Al_{18.6}Si_{77.4}O_{192}$ and $Li_{17.8}K_{0.8}Al_{18.6}Si_{77.4}O_{192}$. TGA analysis was performed as for the zeolite Rho samples.

The crystallinity of all as-prepared, cation-exchanged and calcined samples was confirmed by laboratory PXRD using a Stoe STAD I/P diffractometer using Cu Kα_1 X-radiation (1.54056 Å).

N_2 adsorption isotherms were measured volumetrically at 77 K using a Micromeritics Tristar II 3020. CO_2 adsorption isotherms were measured volumetrically starting at lower pressures using a Micromeritics 2020 porosimeter. This was typically performed from 0 to 1 bar at 298 K, although for Na-Rho isotherms up to 0.14 bar were also collected sequentially on the same sample at 273, 298, and 308 K. Prior to N_2 and CO_2 adsorption/desorption isotherms being measured, the samples were degassed under high vacuum at temperatures chosen from examination of the TGA plots that would result in the removal of all physically bound water. The temperature of 623 K was used for all samples except NH_4-Rho, which is known to undergo partial deammoniation at this temperature. For NH_4-Rho, 500 K was chosen as a compromise temperature to remove most of the physisorbed water while resulting in minor amounts of deammoniation. Indeed, prolonged evacuation at 500 K removed H_2O from all except the Li-forms of the zeolites. During measurement of the CO_2 adsorption isotherms each measurement on the adsorption and desorption branches was allowed up to 2.5 h to reach equilibrium, if this time was required. Ethane adsorption isotherms were measured volumetrically at 293 K using a custom-built glass line.

IR spectra of samples with and without adsorbed CO_2 were measured at room temperature on self-supporting wafers (~30 mg, 2 cm^2) placed in a pyrex cell with KBr windows using a Nicolet Magna instrument (DTGS detector, 4 cm^{-1} resolution). The infrared cell was connected to a vacuum line for evacuation and dehydration. The wafers were heated at 673 K for 4 h to ensure full dehydration, and CO_2 (BOC, SFC grade, >99.9995%) was admitted to give a range of equilibrium pressures.

For all Na,H-Rho samples the reversible capacity for CO_2 adsorption at 0.1 bar CO_2 and at 308 K was estimated by the ZLC method.[16−19] The technique is based in following the desorption curve of a sample previously saturated with a mixture of 10% CO_2 (sorbate) in He (carrier). When equilibrium between the gas phase and the adsorbed phase is reached, the flow is switched to pure He (purge) and the outlet gas phase concentration from the column is monitored. An online quadrupole mass spectrometer (Ametek Benchtop) is connected to the ZLC to monitor the outlet gas concentration. The apparatus is provided with drying columns to ensure predried gases entering the system; high and low flow rate mass flow controllers (0−50 mL/min and 0−3 mL/min, respectively) allowed experiments to be conducted under kinetic and equilibrium control. A very small amount of material (*ca.* 10 mg) is required to fill a ZLC. Before each experiment the samples were dehydrated overnight at 623 K under flow of pure He. The calculations of the CO_2 capacities are based on the dry weight of the sample. To ensure that full saturation was reached, preliminary ZLC experiments were run increasing the exposure time to the sorbate: the sample was fully equilibrated when the CO_2 capacity obtained did not change with the exposure time. Na,Cs-Rho registered the higher saturation time, 5 h; all the Na-Rho samples were saturated for 3 h.

Diffusion measurements at 308 K were performed via analysis of desorption curves obtained by ZLC on Na,Cs-Rho and Na-Rho following equilibration in 10% CO_2 (full saturation) or partial saturation in flowing 10% CO_2 for a shorter time (5.6 min for Na,Cs-Rho, 9.3 min for Na-Rho). In order to confirm the nature of the diffusion process over Na-Rho, experiments were also performed for Na-Rho at 308 K following saturation in 1% CO_2. Further details about the technique and the interpretation of the results are given in section 3.3.6 and in the Supporting Information.

In order to measure the structure of dehydrated zeolites, the powders were loaded into 0.7 mm quartz glass capillaries and dehydrated at 623 K at 10^{-5} mbar on a glass line for 12 h. The powder diffraction patterns of samples were measured in Debye−Scherrer geometry on a Stoe STAD i/p diffractometer with monochromated Cu Kα_1 X-rays (λ = 1.54056 Å). The structures were determined by Rietveld refinement against the XRD data, using the GSAS suite of programs.[31] For zeolite Rho, starting framework models were adapted from literature examples with the unit cell modified to that derived from the diffraction pattern. Starting cation positions were estimated from literature models and the framework atomic positions were refined with geometric constraints on Al,Si−O and O−O distances to maintain regular tetrahedral coordination. Final extra-framework cation positions and occupancies were determined by refinement of starting positions and by using difference Fourier methods to look for additional positions. ZK-5 was similarly refined from a starting model.[20] The ZK-5 prepared here contains a small amounts of chabazite (a polytype of ZK-5), so that the diffraction data was analyzed via a two-phase refinement, using a structural model for chabazite as a starting point.[32] Around 10% of the material was found to be chabazite.

For the fully exchanged sodium form of zeolite Rho, written Na-Rho, the structural response to CO_2 adsorption was measured by *in*

Table 1. Comparison of N_2 Uptake at p/p_o = 0.1 bar, 77 K and CO_2 Uptake at 0.1 and 0.8 bar at 298 K for a series of Rho and ZK-5 Structures of Different Compositions

sample name	unit cell formula of dehydrated sample	N_2 uptake at 0.1 bar, 77 K (mmol g^{-1})	adsorption CO_2 uptake at 0.1 bar, 298 K (mmol g^{-1})	adsorption CO_2 uptake at 0.8 bar 298 K (mmol g^{-1})
Na,Cs-Rho	$Na_{6.8}Cs_{3.0}$ $Al_{9.8}Si_{38.2}O_{96}$	0.27	2.25	3.55
NH_4-Rho	$(NH_4)_{9.8}Al_{9.8}Si_{38.2}O_{96}$	0.20	1.15	4.11
H-Rho	$(AlO_xH_y)_{0.6}H_{9.3-\delta}Al_{9.3}Si_{38.7}O_{96}$	10.5	1.63	3.97
H-SAPO(RHO)	$H_5Al_{24}Si_5P_{19}O_{96}$	10.4	0.98	3.29
US-Rho (743 K)	$(AlO_xH_y)_{5.4}Al_{4.6}Si_{43.4}O_{96}$	9.36	0.92	2.70
Cs-Rho	$Cs_{9.8}Al_{9.8}Si_{38.2}O_{96}$	0.12	0.07	0.53
Na-Rho	$Na_{9.8}Al_{9.8}Si_{38.2}O_{96}$	0.16	3.07	4.23
K-Rho	$K_{9.8}Al_{9.8}Si_{38.2}O_{96}$	0.13	1.50	4.50
Li-Rho	$Li_{9.8}Al_{9.8}Si_{38.2}O_{96}$	0.30	3.36	4.96
Na-ZK-5	$Na_{16.6}K_2Al_{18.6}Si_{77.4}O_{192}$	5.81	4.05	4.81
Li-ZK-5	$Li_{17.8}K_{0.8}Al_{18.6}Si_{77.4}O_{192}$	7.08	4.67	6.09

situ synchrotron X-ray diffraction performed at beamline I-11 at the Diamond Light Source.[33] This was achieved using a custom-built gas handling line.[34] Sample was loaded into a 0.7 mm quartz glass capillary to a depth of around 1 cm, and a quartz wool plug was packed above this to prevent loss of powder upon evacuation and dehydration. The capillary was attached to a gas dosing line attached to a goniometer head, which was permitted to rock by 20° in the beam to improve powder averaging during diffraction. The sample was dehydrated under evacuation (10^{-5} mbar) using an Oxford Cryosystems Cryostream (700 plus) blowing hot air at 500 K for 2 h, under which conditions the sample was observed to have transformed to the dehydrated *I*-43*m* phase. Series of diffraction patterns, each of 2 min and over the 2θ range of 2−140°, were collected at 298 K before and after dehydration and also after dosing with 0.1 and 0.2 bar CO_2, each time after 15 min equilibration. Subsequently, diffraction patterns were measured during evacuation of the sample at 298 K, as carbon dioxide was removed. For the dehydrated zeolite and that on which CO_2 was adsorbed at 0.1 and 0.2 bar, five patterns were summed and the data binned to 0.005(2θ). For other patterns, the data in individual patterns was binned to 0.005(2θ). Full Rietveld refinement was then performed for Na-Rho after dehydration, in equilibrium with 0.1 and 0.2 bar CO_2, and after prolonged evacuation, in each case to determine the framework zeolite structure and the location and site occupancy of sodium cations and any CO_2 molecules. CO_2 adsorption sites were located by difference Fourier mapping. The starting framework model used was that refined against the synchrotron XRD data collected immediately prior to the CO_2 loading. The occupancy and location of the cations and the identified CO_2 positions were then refined against the data with constraints applied to maintain a linear CO_2 geometry and chemically reasonable bond lengths.

3. RESULTS AND DISCUSSION

3.1. Overview of Preparation, Structure, and Adsorption Properties. Rho and ZK-5 zeolites were prepared by hydrothermal synthesis according to the literature.[21,24] For zeolite Rho, the synthesis gave 2 μm particles built up from smaller crystallites around 0.1 μm in size. Zeolite ZK-5 formed as 1.4 μm cubes. Series of Rho and ZK-5 zeolites were prepared by extensive cation exchange and calcination as described in the Experimental Section. Their unit cell compositions were estimated from a combination of EDX and MASNMR analysis. The Si/Al ratio measured in the as-prepared zeolite Rho was measured by EDX as 4.0 and by deconvolution of the ^{29}Si spectrum as 3.9. The latter value was taken as the more accurate, and compositions calculated accordingly for both Rho and ZK-5 materials. Full details of the composition of cation-exchanged zeolites are given in Table 1. These assume full charge balance by univalent cations, and EDX measurements are within experimental error of this.

The H-form was prepared by deammoniation of NH_4-Rho under shallow bed heating. The bulk Si/Al ratio was not affected, but the framework Si/Al was shown by ^{29}Si MASNMR to have increased slightly (to 4.15) and ^{27}Al MASNMR indicated the presence of a small amount of octahedrally coordinated and therefore presumably extra-framework aluminum species corresponding to a loss of *ca.* 0.5 Al^{3+} per unit cell from the framework. The charge balance for the framework Al^{3+} is attributed to protons. Indeed, previous neutron diffraction studies of deammoniated Rho have located bridging hydroxyl groups in the structure.[30]

We were also interested in the effect on CO_2 adsorption of framework dealumination of the Rho structure during steaming, in which hydrothermal treatment of the NH_4-Rho results in migration of tetrahedrally coordinated framework Al to extra-framework positions and recrystallization of the framework with a higher Si/Al ratio. For all steamed samples (at 743, 773, and 823 K) the framework Si/Al ratio was the same (within the limits of accuracy) at 9.4. This indicates a framework Al content of 4.6 per unit cell, and therefore a loss of *ca.* 5.4 Al per unit cell during deammoniation. The coordination geometry of the extra framework Al was investigated by a combination of ^{27}Al MASNMR and MQ MASNMR (Figure 2). Aluminum removed from the framework is observed to move to extra-framework sites that can be 4-, 5-, or 6-fold coordinated, behavior very similar to that reported for Al^{3+} cations in dealuminated zeolite Y.[35] It was not possible to exchange any of this extra-framework aluminum. The only effect of higher steaming temperatures was to reduce the pore volume, so that the results presented in Table 1 are for the sample steamed at 743 K.

For each of the Rho materials, PXRD of the dehydrated samples were measured at 298 K, and the structures were refined by Rietveld analysis as described in the Experimental Section. Crystallographic details are given in Table 2, including the minimum O···O distance across the elliptical (or circular) windows delimited by 8MRs and calculated from the distance between the O atom centers, minus twice the ionic radius of O^{2-}, 1.35 Å. It should be noted that Cook and Conner[36] suggest that the effective pore size of zeolites is consistently 0.7 Å more than that usually quoted on the basis of this hard sphere model, especially when comparing these values with Lennard-Jones radii (2.98 Å for the smaller dimension of CO_2

dx.doi.org/10.1021/ja3070864 | J. Am. Chem. Soc. 2012, 134, 17628−17642

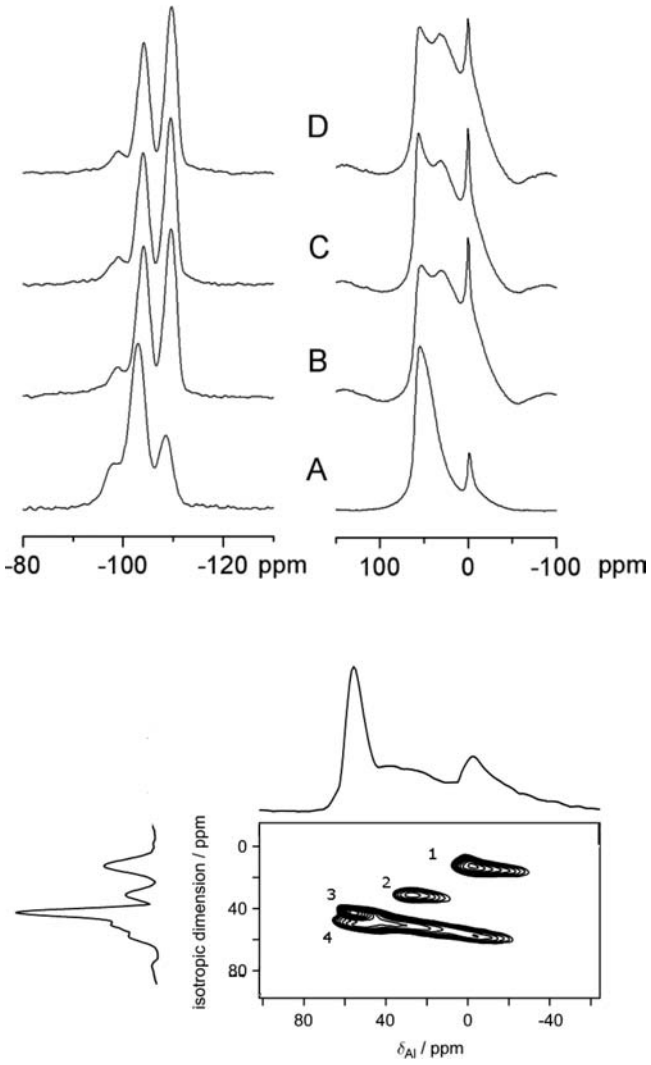

Figure 2. (Top) (left) ^{29}Si and (right) ^{27}Al MASNMR of NH_4-Rho (A) heated at 773 K in dry N_2 flow and steamed at (B) 743 K, (C) 773 K, and (D) 823 K. (Bottom) 3Q ^{27}Al MASNMR of sample steamed at 743 K: 1, octahedral Al in extra-framework positions; 2, five-coordinate Al in extra-framework positions; 3, tetrahedral framework Al; 4, Al in a distorted tetrahedral extra-framework environment.

via a 2-center Lennard-Jones model[37]). This difference between crystallographic values using ionic radii and empirical observations is attributed to thermal motion, chemical interaction, and the difference in the type of atomistic model. The occupancy of the cation sites, defined as types I, II, and III as described below, are also given in Table 2, with full details of the atomic coordinates supplied in the Supporting Information.

For all Rho zeolites in the hydrated form the structure adopts the centrosymmetric structure. Upon dehydration H-Rho remains centrosymmetric (*Im*-3*m*), whereas for all cation-exchanged Rho materials dehydration resulted in transformation to the noncentrosymmetric *I*-43*m* form. Univalent cation positions were located within the center of the double eight ring window site, D8R (coordinates (1/2,0,0) denoted site I here), at a site close to the plane of the 8MR (S8R site, coordinates (x,0,0), $x \approx 0.4$, denoted site II), or at sites close to 6MRs in the α-cage (S6R, coordinates (x,x,x), $x \approx 0.2 - 0.3$, denoted site III). These sites are consistent with those reported in the literature and are illustrated in Figure 3 for Na,Cs-Rho, Na-Rho, Cs-Rho, NH_4-Rho, Li-Rho, and K-Rho, showing for each a possible arrangement of cations in a single cage. The cation occupancies given in Table 2 are those from unconstrained refinement. Differences from the expected 9.8 cations per unit cell are thought to derive from inherent uncertainties in refinement against laboratory XRD data.

Although cation rearrangement is possible upon CO_2 uptake, as observed by Palomino et al. in Na,Cs-Rho,[9] these framework structures and cation positions are a good starting point for understanding the adsorptive properties of Rho as the solid is first put in contact with CO_2. The structures are described below for H-forms of Rho and related solids; Na,Cs-, Na-, and Cs-forms; and the other cation forms (NH_4, Li, K). In addition, the cation location in a partially exchanged Na,H-Rho is also given in Table 2.

The structure of cation-exchanged zeolites Na- and Li-ZK-5 were also determined by Rietveld refinement, taking into account the residual K^+ in these materials and also the presence of chabazite impurity. Two extra-framework cation site locations were located for Na^+ cations. The first type is in strongly nonplanar 8MRs of the PAU cages between α-cages (Type 1 in Table 3), whereas the second is in 6MRs of the α-cages (Type 2 in Table 3). For Na-ZK-5 the Na−O distances in the 8MR sites are 2.67(1) Å and for the 6MR are 2.35(1) Å. In Li-ZK-5 the 6MR sites are fully occupied by Li^+ cations, and there is some scattering (assigned as K^+) in the 8MR sites. The Li−O distances in the 6MR sites are 2.09(1) Å, as expected, and the K−O distance is 2.89(1) Å. The locations are

Table 2. Space Group, Minimum O−O Distance of 8MR Windows, and Cation Site Occupancies in Dehydrated Zeolite Rho (Site I, D8R; Site II, S8R; Site III, S6R)[a]

				site I		site II		site III	
sample	unit cell parameter (Å)	space group	O···O (Å)	frac occup	atoms/unit cell	frac occup	atoms/unit cell	frac occup	atoms/unit cell
Na,Cs-Rho	14.5307(4)	*I*-43*m*	2.69	0.4258(25)	2.55(2)	0.252(11)	3.02(13)	0.317(18)	2.54(14)
NH_4-Rho	14.7018(2)	*I*-43*m*	2.85	0.323(6)	1.93(4)	0.677(6)	8.12(7)		
H-Rho	15.0352(2)	*Im*-3*m*	3.88						
Na-Rho	14.3771(2)	*I*-43*m*	2.26			0.539(7)	6.47(8)	0.372(11)	2.98(9)
Na-Rho (50%)	14.3447(2)	*I*-43*m*	2.21	0.269(6)	1.61(4)	0.241(3)	2.89(4)		
Li-Rho	14.2448(2)	*I*-43*m*	1.90					1.00	8.00
Li-Rho (50%Li)	14.4239(5)	*I*-43*m*	2.24					0.65(3)	5.20(24)
K-Rho	14.5951(2)	*I*-43*m*	2.72	0.343(4)	2.06(2)	0.571(3)	6.85(4)		
Cs-Rho	14.5947(3)	*I*-43*m*	2.85	1.00	6.00			0.424(3)	3.39(2)

[a] As determined by Rietveld refinement from laboratory powder X-ray diffraction collected at 293 K.

dx.doi.org/10.1021/ja3070864 | J. Am. Chem. Soc. 2012, 134, 17628−17642

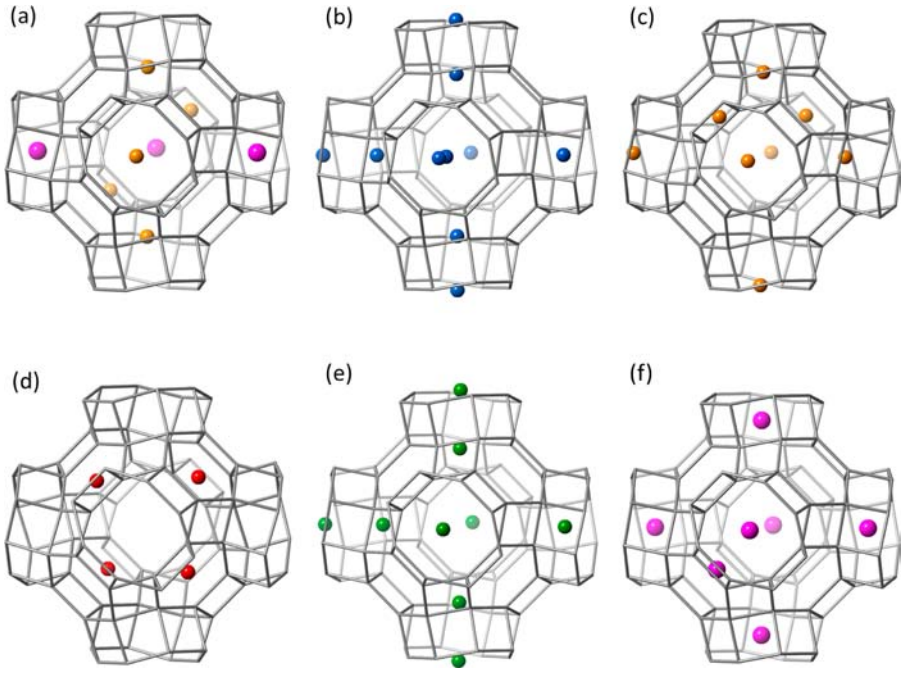

Figure 3. Possible cation distributions in one α-cage and associated D8R windows of dehydrated univalent cation forms of zeolite Rho, determined from Rietveld refinement of laboratory X-ray powder diffraction data. (a) Na,Cs-Rho (larger spheres, Cs; smaller spheres, Na), (b) NH_4-Rho (N only represented), (c) Na-Rho, (d) Li-Rho, (e) K-Rho, (f) Cs-Rho.

Table 3. Refined Unit Cell Parameters, Window Size, Cation Locations, and Occupancies in Na-ZK-5 and Li-ZK-5 of Table 1[a]

				8MR site occupancy		6MR site occupancy	
sample	unit cell parameter (Å)	space group	O···O (Å)	frac occup	cations/unit cell	frac occup	cations/unit cell
Na-ZK-5	18.6142(2)	*Im*-3*m*	4.00	0.166(1) K	1.99(2) K	0.536(4) Na	8.57(6) Na
				0.636(5) Na	7.63(5) Na		
Li-ZK-5	18.5985(3)	*Im*-3*m*	3.90	0.089(5) K	1.08(1) K	1 Li	16 Li

[a]Obtained by Rietveld analysis of laboratory X-ray data collected at 293 K.

illustrated for Na-ZK-5 in Figure 4, which shows that the 8MR windows between cages do not have cations in them and have O···O distances (taking ionic radii into account) of 4.0 Å.

3.2. CO_2 Adsorption Performance of Different Univalent Cationic Forms of Zeolite Rho Related to Their Dehydrated Structures. *3.2.1. CO_2 Adsorption on the H-Form of Zeolite Rho and Related Materials.* Although none of the materials was cation-free, the closest estimate of the intracrystalline pore volume of an "empty" framework can be made by considering adsorption on the protonic form. H-Rho possesses a pore volume of 0.36 $cm^3\ g^{-1}$ (10.5 mmol(N_2) g^{-1}), and H-Rho has previously been shown to possess Brønsted acid sites.[38] H-zeolites are known in general to show weaker electrostatic effects than cationic forms, due to the polarizing effect of the protons in the bridging hydroxyl groups. As a result, the uptake of CO_2 at 298 K and 0.1 bar on H-Rho is relatively low (1 mmol g^{-1}) due to the weak interactions (Figure 5). This uptake increases to 3.5 mmol g^{-1} by 0.9 bar and is fully reversible. The structure of dehydrated H-Rho was confirmed to have *Im*-3*m* symmetry, a = 15.0352(2) Å, where the circular 8-rings have an opening large enough to admit both N_2 and CO_2. Notably, the isotherm is very different from that reported by Araki et al. for the so-called H-Rho of their work.[11] The difference arises because at their lower ion exchange temperature not all of the Cs^+ is exchanged by ammonium and the non-Type I isotherm shape probably results from a structural change occurring as P_{CO_2} increases, controlled by the presence of the residual Cs^+ cations in D8R sites.

The calcined, dehydrated H-SAPO(RHO) structure has been reported previously in the *I*23 space group, to permit ordering of Al and P (and Si, which substitutes for P).[39] The window size of the dehydrated solid is large enough to permit uptake of N_2 and CO_2. Direct comparison of the CO_2 isotherm of H-SAPO(RHO), consistent with those reported elsewhere,[40] with H-Rho, indicates that H-SAPO(RHO) is a weaker adsorbent (Figure 5). The overall anionic charge on the framework in the SAPO form is lower than that of the aluminosilicate, so that there will be less electrostatic interaction.

The N_2 uptake of steamed (ultrastabilized) zeolite Rho at 0.1 bar at 77 K (9.6 mmol g^{-1}) was close to that of the H-Rho, but CO_2 adsorption at 0.1 bar and 298 K is lower, indicating that there is a weaker interaction. That there is no strong interaction with the extra framework aluminum species indicates that the trivalent Al^{3+} cations must be shielded by associated hydroxide and/or oxide species, either within the cages, or in their own nonporous alumina phase. The observed weaker interaction is attributed to the lower framework charge in the dealuminated framework.

3.2.2. CO_2 Adsorption Related to Structure for Na,Cs-, Na-, and Cs-Rho. Na,Cs-Rho showed no N_2 adsorption at 77 K, but appreciable CO_2 uptake at 298 K (Table 1 and Figure 6), with significant hysteresis observed under the conditions of the

dx.doi.org/10.1021/ja3070864 | J. Am. Chem. Soc. 2012, 134, 17628−17642

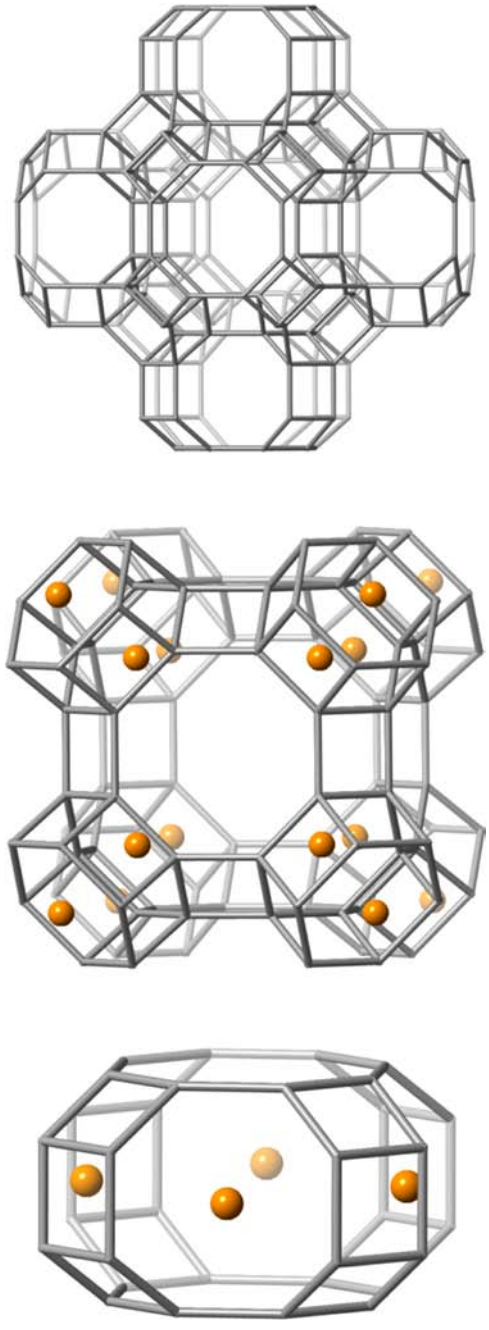

Figure 4. (Top) Framework structure of ZK-5 with O atoms omitted for clarity and T−T linkages represented by gray sticks, showing α-cage surrounded by six *pau* cages (which lead to six other α-cages). (Middle) Type 1 cations in 6MR sites in α-cage. (Bottom) Type 2 cations in puckered 8MR sites in *pau* cage.

measurement of the adsorption isotherm (max 2.5 h equilibration time). In this structure, when dehydrated, around one-half of the D8R sites are occupied by Cs^+ while Na^+ cations occupy sites of type II near the 8MRs in other windows of the large α-cages (Figure 2). That CO_2 is adsorbed must indicate that either the Cs^+ or the Na^+ cations (or both) must be able to move to permit diffusion. The *in situ* XRD structural studies of Palomino et al.[9] indicate that above 1 bar at 298 K the structure changes symmetry to *Im*-3*m* and that at 5 bar Cs^+ is displaced from its position in site I to occupy a position at site II. The adsorption data here confirms that some cations must move

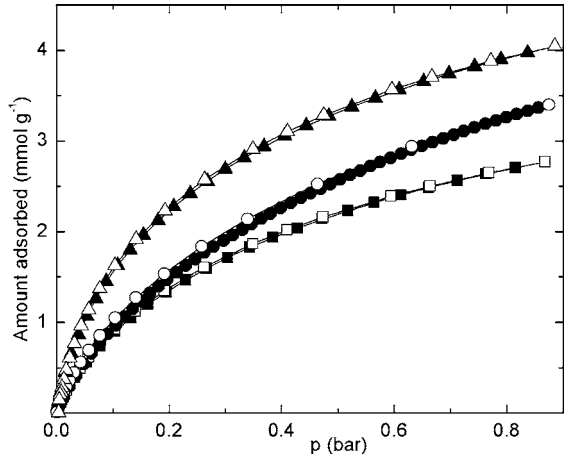

Figure 5. CO_2 isotherms at 298 K for H-Rho (triangles), US-Rho (squares), and the H-form of SAPO(RHO) (circles). Adsorption, closed symbols; desorption, open symbols.

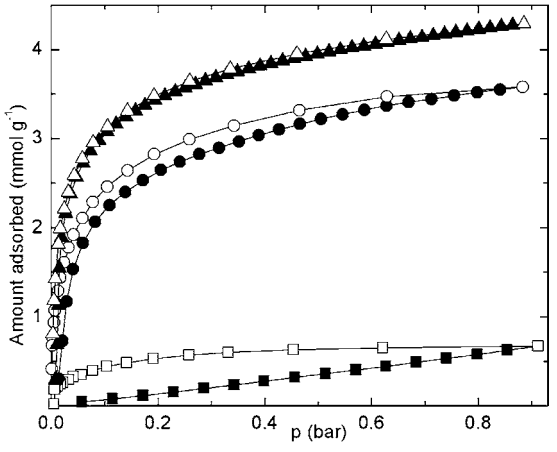

Figure 6. CO_2 isotherms at 298 K for Na,Cs-Rho (circles), Na-Rho (triangles), and Cs-Rho (squares). Adsorption, closed symbols; desorption, open symbols.

sufficiently far away from their S8R site to permit the CO_2 molecules to enter the cage.

To determine the relative mobility of Cs^+ and Na^+ in these window sites, the pure Na^+ and Cs^+ cation forms were prepared, and the structures of the dehydrated cationic forms were measured by Rietveld refinement of laboratory X-ray data (Table 2). In each case, the dehydrated form distorts to the noncentrosymmetric *I*-43*m* structure, with different unit cell parameters and 8MR openings. In Cs-Rho the cations fully occupy the D8R sites and also occupy S6R (type III) sites within the α-cages. In Na-Rho the cations occupy S8R sites as well as some S6R (type III) sites, so that each window has a cation at site II, assuming that two Na^+ cations will favor being distributed over two D8R windows rather than occupying two sites in one and none in another. This is supported by the observation of Na^+ cations in S6R sites as soon as there are enough cations per unit cell to exceed one per window (observed in Na-Rho, Na,Cs-Rho). In neither Cs- nor Na-Rho was N_2 adsorbed at 77 K, due to the blocking action of the cations, further supporting evidence for Na^+ cations in all D8R windows. Adsorption isotherms at 298 K up to 1 bar show the Cs^+ form adsorbs only low amounts of CO_2, whereas the Na-form adsorbs CO_2 strongly, even at low partial pressures (3.2

dx.doi.org/10.1021/ja3070864 | J. Am. Chem. Soc. 2012, 134, 17628−17642

mmol g^{-1} at 0.1 bar) (Figure 6) even though the window size in Na-Rho (neglecting cations) is smaller than that in Cs-Rho. Na-Rho adsorption and desorption isotherms show relatively little hysteresis at most of the pressures under these conditions of measurement, although more careful examination (see section 3.3.2) showed significant hysteresis at low pressures. Comparing these results, we conclude that at $P < 1$ bar the Cs^+ cations in D8R sites block the windows and also that diffusion of CO_2 into and through Na,Cs-Rho must occur largely through the 8MR windows occupied by Na^+ cations. The uptake on the Na-form is considerably higher than on the H-form at comparable pressures, as a result of the increased electrostatic interaction.

3.2.3. CO_2 Adsorption Related to Structure for NH_4-, Li-, and K-Rho. Additional univalent cation forms of zeolite Rho were prepared to determine the effects of different univalent cations on CO_2 adsorption on zeolite Rho. These were, in order of increasing cationic radius, Li^+, K^+, and NH_4^+. For Li-Rho, the low atomic number of lithium makes determination of the lithium site occupancies difficult, but significant scattering was measured at the S6R sites, corresponding to between 5 and 6 Li^+ cations. This is unlikely to be an accurate value due to the low electron density of Li^+ but a previous structural analysis by neutron diffraction of a dehydrated mixed Li,Na,Cs-aluminosilicate zeolite indicated that the S6R site is the preferred position for the small Li^+ cation.[15] It is therefore probable that most of the Li^+ cations required for charge balance are located in this site and not in the window sites. In K-Rho, by contrast, K^+ cations are found to occupy window sites of both S8R and D8R types so that there will be at least one and in some case two K^+ cations per window (which would in the latter case occupy two S8R sites 4.0 Å apart). Available structural data on ammonium forms of Rho by neutron and X-ray diffraction indicate that at high ammonium contents (12 per unit cell) the cations occupy S8R sites upon dehydration, whereas partially deammoniated samples with 6 NH_4^+ per unit cell the cations occupy D8R sites.[29,41] For the sample measured here it is likely that NH_4^+ cations occupy both D8R and S6R sites in a similar way to K^+ in K-Rho.

None of these forms of zeolite Rho adsorbed N_2 at 77 K. For K- and NH_4-Rho, as for its Na- and Cs-forms, the very low uptake of N_2 at 77 K is due to cations blocking window sites and not being mobile at the low temperature. For Li-Rho the window size is the more important parameter because Li^+ cations do not occupy window sites, but even at room temperature the narrowest O···O window opening is only 1.9 Å. In Li-Rho the strong distortion away from *Im*-3*m* results as the 6MRs distort to afford the small Li^+ cations better coordination in type III sites (rather than due to distortion of the 8MRs to give better coordination to cations in sites I and/or II as is the case for the other cation forms).

To investigate further the effect of Li^+ ions on adsorption onto Li-Rho, N_2 adsorption was measured on samples with different Li^+ contents (Supporting Information). Adsorption decreased steadily above 2 Li^+ per unit cell, from a maximum of 10.4 mmol g^{-1}, to negligible amounts at full exchange. As Li^+ cations are located mainly at the S6R sites the decrease in uptake is due to the decrease of the window size that results from the framework distortion. At room temperature, for example, the O···O distance (taking ionic radii into account) is already reduced to 2.24 Å by the presence of 5 Li^+ per unit cell.

Li-, K-, and NH_4-Rho, like Na-Rho, all adsorb CO_2 at 298 K, as shown in Figure 7. CO_2 adsorption onto Li-Rho gave very high uptakes, even at low partial pressures. Also, the adsorption was Type I in character. Most of the Li^+ cations are in the S6R sites, leaving the window sites empty. The CO_2 is small enough to pass through the open windows of the dehydrated Li-Rho structure, even though the crystallographic distance is apparently too small (1.9 Å), suggesting that the framework is flexible locally at 298 K.

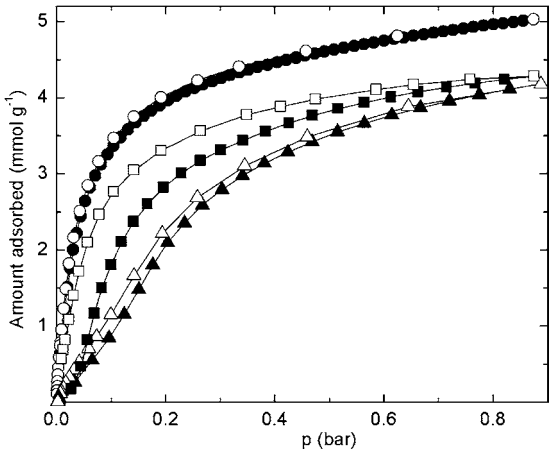

Figure 7. CO_2 isotherms at 298 K for Li-Rho (circles), K-Rho (squares), and NH_4-Rho (triangles). Adsorption, closed symbols; desorption, open symbols.

The adsorption and desorption branches of NH_4-Rho show relatively little hysteresis, but the uptake at 0.1 bar is not as high as that observed for the Na^+ form. This indicates that the ammonium ions must be able to move from their position within the D8R windows to allow diffusion through the windows. The lower uptake may partly be because the sample was not heated above 493 K under vacuum, to avoid deammoniation, and so might have some residual physically adsorbed water, but it is likely that the electrostatic interaction between the CO_2 and the NH_4^+ cations is weaker than that with the smaller Na^+ cations.

By comparison with Na-Rho and NH_4-Rho, adsorption and desorption isotherms on the K-form of zeolite Rho show much more marked non-type I behavior and hysteresis, even with equilibration times of 2 h. Nevertheless, high uptakes at partial pressures approaching 1 bar are achieved. Since all K^+ cations in K-Rho occupy sites either in the D8R position or in S8R sites on either face of the window, the K^+ cations must move to allow CO_2 uptake. The observed hysteresis results from the need for the movement of K^+ cations to allow passage of the CO_2 molecules: this must be energetically more difficult than movement of the Na^+ cations, possibly because it must move from D8R sites rather than S8R sites, and the former have coordination from more O atoms.

To further confirm that it is the displacement of the K^+ cation that inhibits the CO_2 adsorption, rather than a molecular sieving effect due to distortion of the 8MR away from circular, comparison of the minimum ring distance (Table 2) in the Na- and K-Rho indicates that this is smaller for the Na-Rho than for the K-Rho, but hysteresis is greater for the K-Rho. As previously discussed, for the Li-Rho the distance is smaller still, but no hysteresis is observed because Li^+ cations are not present in the window sites.

3.2.4. CO_2 Adsorption Related to Structure for Li- and Na-ZK-5. To examine the role of structure type on adsorption, CO_2 isotherms were also collected at 298 K on the Li- and Na-forms

dx.doi.org/10.1021/ja3070864 | J. Am. Chem. Soc. 2012, 134, 17628−17642

of ZK-5 of similar framework composition to the Rho material (Supporting Information). The ZK-5 materials have permanent porosity for N_2 (Table 1), and for CO_2 adsorption no hysteresis was observed and high uptakes were achieved at 0.1 bar (Li-ZK-5, 4.67 mmol g^{-1}; Na-ZK-5, 4.05 mmol g^{-1}), comparable to values reported for its polytype chabazite.[4,5] The framework structure of ZK-5 contains α-cages (as found in zeolite Rho) but linked via larger paulingite *pau* cages (Figure 4). In Na-ZK-5 the Na^+ cations occupy sites either within strongly nonplanar 8MR sites in these *pau* cages, which do not block access between α-cages, or in 6MR sites within the α-cages themselves, whereas in Li-ZK-5 most of the Li cations occupy 6MR sites. Direct comparison of the adsorption behavior of Na-ZK-5 with that of Na-Rho confirms that the hysteresis observed over Na-Rho is not due to the interaction of CO_2 with the cations, but rather due to their effect when occupying sites in the distorted 8MR windows connecting the α-cages. More detailed adsorption data on different cationic forms of ZK-5 (Si/Al = 4.7) published very recently confirm the levels of CO_2 uptake described here.[42]

3.3. Detailed Examination of CO_2 Adsorption on Sodium Rho. Of the different cation forms of Rho examined, the Na-form was chosen for more detailed investigation. Although the Li-form has higher CO_2 uptakes, the lower cost and lower affinity for water of the Na-form would be practical advantages. Furthermore, Na-Rho shows appreciable uptake at 0.1 bar, 298 K (at 3.2 mmol g^{-1} this is the same as that observed for Na-13X under the same conditions, Supporting Information) and the presence of Na^+ cations in window sites leads to hysteresis, which is unusual for zeolites. The related Na,Cs-Rho shows high selectivity for CO_2 compared to other larger, nonpolar molecules (CH_4), as illustrated by Palomino et al.,[9] so it was also of interest to investigate the uptake of Na-Rho for small hydrocarbons. Finally, adsorption of CO_2 was faster and uptake higher on Na-Rho than on K-Rho, and so more likely to be useful in processes requiring successive adsorption and desorption cycles. For these reasons, the mechanism of CO_2 adsorption on Na-Rho was studied in more detail. The additional studies included (i) examination of the adsorption properties of a series of Na,H-Rho samples with varying Na^+ content; (ii) measurement of high resolution, low P_{CO_2} adsorption/desorption isotherms on Na-Rho at different temperatures; (iii) *in situ* synchrotron X-ray diffraction during CO_2 adsorption and desorption on Na-Rho; (iv) *in situ* IR spectroscopy of CO_2 adsorption on Na-Rho and other cationic forms; (v) adsorption of ethane; and (vi) ZLC analysis to give details on the kinetics of CO_2 desorption on Na-Rho. Together, these experiments give an atomistic and quantitative description of the mechanism by which CO_2 is adsorbed and desorbed from zeolite Na-Rho.

3.3.1. N_2 and CO_2 Adsorption on Partially Exchanged Na,H-Rho. Examination of the N_2 capacity at 77 K and reversible CO_2 uptake at 300 K and 0.1 bar, measured by ZLC, of a series of Na,H-Rho materials of different cation contents (Figure 8) shows that by the inclusion of 4 Na^+ cations per unit cell the permanent porosity to N_2 at 77 K is reduced to zero. Furthermore, when reversible CO_2 adsorption measurements are made on Na,H-Rho with variable Na^+ content, there is only a small increase in the amount of reversibly bound CO_2 measured at 0.1 bar by ZLC as the number of Na^+ cations is increased up to 4, but at 6 cations per unit cell and above the uptake increases as the sodium content increases.

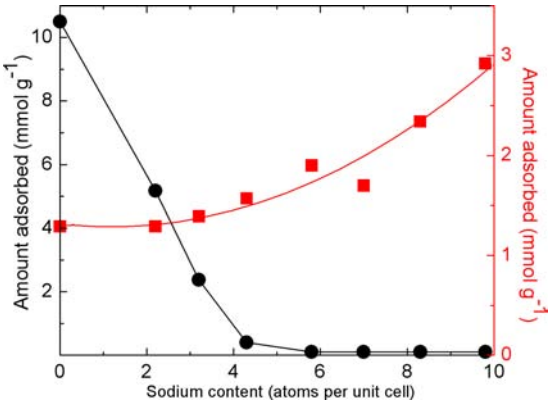

Figure 8. Uptake of N_2 at pore filling at 77 K (left) and reversible CO_2 adsorption measured by ZLC at 308 K (right) as a function of Na content in Na,H-Rho.

These observations are partially explained by reference to the structural analyses of a Na,H-Rho containing 4.9 Na^+ cations per unit cell and of fully exchanged Na-Rho (Table 2). At this level of Na^+ cations per unit cell, the sodium cations occupy almost all of the windows, distributed over sites I and II. It is likely that they are not mobile at 77 K so that there are no easy routes for N_2 through the pore space. They are mobile at 298 K in the presence of CO_2, permitting uptake, but there are few strong adsorption sites at this Na^+ level. At higher Na^+ contents the S6R sites become occupied, and the presence of additional cations in these S6R sites results in the creation of more energetic sites for CO_2 adsorption.

3.3.2. Variable Temperature CO_2 Adsorption/Desorption Isotherms. The Na-Rho CO_2 adsorption/desorption isotherms at 273, 298, and 308 K (measured up to 140 mbar) show strong deviation from Type I behavior at low pressure, and strong hysteresis in the desorption branch (Figure 9). The CO_2

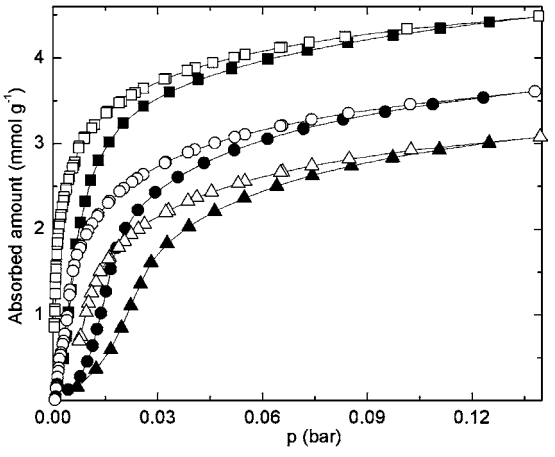

Figure 9. CO_2 isotherms up to 140 mbar for Na-Rho at 273 K (squares), 298 K (circles), and 308 K (triangles). Adsorption, closed symbols; desorption, open symbols.

adsorption behavior of Na-Rho lies intermediate between that of Li-Rho, which shows a type I isotherm with very little hysteresis (Figure 7), and that of K-Rho, which shows more strongly pronounced deviation (Figure 7). Hysteresis and non-type I isotherms suggest that there is a structural change and/or dynamic effects during the adsorption, as frequently observed during adsorption on flexible metal organic frameworks,

dx.doi.org/10.1021/ja3070864 | J. Am. Chem. Soc. 2012, 134, 17628−17642

including during CO_2 adsorption.[43] To investigate possible structural changes upon CO_2 adsorption onto Na-Rho, structural studies during the adsorption and desorption process were performed *in situ* by synchrotron PXRD.

3.3.3. In Situ XRD Studies of CO_2 Adsorption. X-ray diffraction patterns were collected on a sample of dehydrated Na-Rho before and after admitting CO_2 to the gas cell at equilibrium P_{CO_2} values of 0.1 and 0.2 bar. Subsequently, the pressure was reduced to 0.045 bar and a diffraction pattern taken at equilibrium, before the gas cell was evacuated and the diffraction pattern measured every 2 min (Supporting Information). Rietveld refinement gives the structures (Figure 10, Table 4, Supporting Information). Hydrated Na-Rho solid

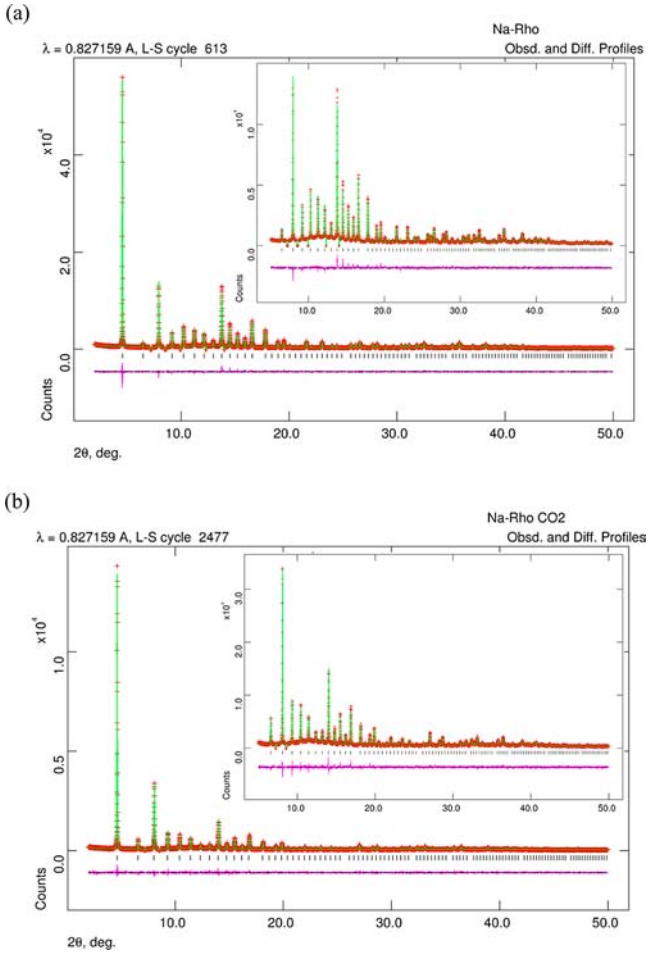

Figure 10. Rietveld plots of synchrotron PXRD profiles (λ = 0.827159 Å, T = 298 K) of (a) Na-Rho (dehydrated) and (b) Na-Rho with CO_2 adsorbed at an equilibrium pressure of 0.1 bar.

has *Im*-3*m* symmetry, a = 14.9573(1) Å, and in the dehydrated state has *I*-43*m* symmetry, with a = 14.4136(3) Å. As observed for the laboratory data, sodium cations occupy S8R sites (*ca.* one cation per window between cages) with *ca.* 2 Na^+ cations in S6R sites in each α-cage (around 1 per two sites). Upon adsorption of CO_2 at 0.1 bar, the unit cell increased to a = 14.6281(7) Å, but the symmetry remained *I*-43*m*. The expected uptake at 0.1 bar on the adsorption branch of the isotherm is 3.1 mmol g^{-1}, corresponding to 9.8 molecules of CO_2 per unit cell. Difference Fourier analysis together with constrained refinement locates two sites for CO_2 molecules in the Na-Rho structure at this point on the isotherm, total occupancy 10.1 molecules per unit cell, one of which resides partly in the D8R and the other fully in the α-cage. Careful examination of the refined positions of the CO_2 molecules, together with those of the Na^+ cations (all at partial occupancy) suggest a likely configuration for CO_2 at the two sites (Figure 11). In the first location (A) the CO_2 molecule adopts end-on coordination with one Na^+ cation in the S8R, with a Na^+—O distance of 2.88(2) Å, through the D8R cage windows to project into the α-cage, where its other O atom is 4 Å from Na^+ cations of type III. Possible disordered canting of the OCO molecules toward the type III cations, which would be difficult to confirm, could reduce that distance. The Na^+ cations in the D8R adjust their position as this adsorption occurs (see Supporting Information) so the crystallographic Na^+—Na^+ distance, at 1.73(1) Å, precludes occupancies above 50% and so supports a model where there is one Na^+ cation per D8R window. In the second location (B) the CO_2 molecule adopts end-on coordination with one α-cage Na^+ cation, with a Na— O distance of 2.58(1) Å, with the second O atom at its closest 4.5 Å from a second α-cage Na^+ cation. Adjacent OCO molecules could align as shown in Figure 11. Two possible arrangements of Na^+ cations and CO_2 molecules in Na-Rho at 298 K in contact with 0.1 bar CO_2 are shown in Figure 12, taking into account possible arrangements of Na^+ cations and CO_2 molecules derived from the refinements. At 0.2 bar CO_2 there is a slight expansion in the unit cell (to 14.6348 Å) as additional CO_2 molecules are adsorbed (total refined content 10.8 per unit cell).

Simulation of adsorption of CO_2 in zeolite Na-A at levels up to 3 molecules per α-cage suggests all CO_2 molecules interact with two (or three) Na^+ cations, and the CO_2 molecules interact most strongly with cations in 6MR and 8MR sites in this solid.[23] The structure reported here, together with the nonlinear increase in strongly bound CO_2 with increasing Na^+ content, suggests 2-cation—CO_2 interactions might also be important in zeolite Rho.

Upon reducing the equilibrium pressure to 0.045 bar, there is a small reduction in the unit cell parameter (to 14.6219 Å) and the refined site occupancies remain similar (the total refined CO_2 occupancy per unit cell drops to 9.8 molecules). This is expected from the shallow desorption branch observed in the low pressure isotherms shown in Figure 9. It is only when the sample is opened to vacuum that the unit cell begins to contract sharply, as the steep part of the desorption branch is descended (Supporting Information). Refinement indicates that already after a few minutes of evacuation the amount of ordered CO_2 in the pores has decreased, but the occupancy of the two sites has not decreased evenly. The CO_2 molecules in site B are held more weakly than those in site A, so that whereas the number in site A drops by 27% (from 6 to 4.4 molecules), that in site B drops by 58% (from 3.8 to 1.6). At any time there is a single phase present, so that changes in the framework must propagate rapidly throughout the crystallites. Only after prolonged evacuation does the unit cell parameter approach that of the empty structure, as a result of slow desorption.

3.3.4. In Situ IR Spectroscopy of CO_2 Adsorption. The *in situ* IR spectroscopy of CO_2 adsorbed on zeolite Na-Rho can be interpreted in the light of the adsorption isotherms and the structural information and also compared with the results on Li-Rho, Na,Cs-, and K-Rho. The infrared spectrum of CO_2 adsorbed on Na-Rho at low coverages showed a single strong band at 2358 cm^{-1} due to the ν_3 asymmetric stretching vibration of adsorbed CO_2. (Figure 13a). This is shifted to

dx.doi.org/10.1021/ja3070864 | J. Am. Chem. Soc. 2012, 134, 17628—17642

Table 4. Atomic Coordinates, Site Multiplicities, Occupancies, and Displacement Parameters for Na-Rho at 298 K, (i) Dehydrated, *I*-43*m*, *a* = 14.4134(1) Å and (ii) in Equilibrium with 0.1 bar CO_2 during Adsorption, *I*-43*m*, *a* = 14.62823(6) Å, Determined by Rietveld Analysis of Synchrotron PXRD

atom	*x*	*y*	*z*	multiplicity	frac occup	U_{iso}/Å^2
			(i) Na-Rho (Dehydrated)			
Si1	0.27429(15)	0.12260(18)	0.42518(17)	48	0.8	0.0132(5)
Al1	0.27429(15)	0.12260(18)	0.42518(17)	48	0.2	0.0132(5)
O1	0.0388(3)	0.2113(2)	0.3868(3)	48	1	0.0045(8)
O2	0.2194(3)	0.2194(3)	0.4039(5)	24	1	0.0045(8)
O3	0.1170(3)	0.1170(3)	0.6275(4)	24	1	0.0045(8)
Na(II)	0.3869(9)	0	0	12	0.5	0.0490(5)
Na(III)	0.3103(8)	0.3103(8)	0.3103(8)	8	0.389(8)	0.0490(5)
			(ii) Na-Rho (0.1 bar CO_2)			
Si1	0.26879(10)	0.11856(12)	0.41920(11)	48	0.8	0.0064(2)
Al1	0.26806(10)	0.11889(12)	0.41992(11)	48	0.2	0.0064(2)
O1	0.0302(2)	0.20921(18)	0.38306(24)	48	1	0.0085(5)
O2	0.2092(2)	0.2092(2)	0.3916(3)	24	1	0.0085(5)
O3	0.1276(2)	0.1276(2)	0.6274(3)	24	1	0.0085(5)
NaIII	0.3084(6)	0.3084(6)	0.3084(6)	8	0.4	0.053(3)
NaII	0.4408(5)	0	0	12	0.5	0.053(3)
OC1	0.3828(7)	0	0	12	0.5	0.053(3)
OC2	0.2306(7)	0	0	12	0.5	0.053(3)
CO1	0.3074(7)	0	0	12	0.5	0.053(3)
OC3	0.3683(7)	0.4863(15)	0.3683(7)	24	0.171(1)	0.053(3)
CO2	0.3489(7)	0.5597(15)	0.3711(18)	48	0.0855(5)	0.053(3)
OC4	0.3206(7)	0.6306(15)	0.3849(18)	48	0.0855(5)	0.053(3)

higher frequency relative to the gas phase molecule (2349 cm^{-1}). A similar shift has been reported for CO_2 adsorbed in Na-ZSM5 and attributed to interaction of CO_2 with the Na^+ cations.[44] A much smaller shift (to 2351 cm^{-1}) is reported for CO_2 adsorbed in NaY,[45] presumably reflecting a weaker interaction.

Direct evidence for a CO_2–Na^+ interaction comes from observation of the ν_1 symmetric stretching vibration of adsorbed CO_2 in Na-Rho as a weak band at 1378 cm^{-1} (Figure 13b). This vibration is infrared forbidden for the gas phase molecule (at 1388 cm^{-1}) but becomes weakly allowed when the symmetry is lowered due to interaction with zeolite cations. Garrone et al.[44] report this frequency to be 1382 cm^{-1} for CO_2 adsorbed in Na-ZSM-5.

As the CO_2 coverage is increased in Na-Rho, the ν_3 band broadens and becomes too intense to monitor. Several weak bands then become evident on either side of this feature, at 2293, 2405, 2450, and 2503 cm^{-1}. The 2293 cm^{-1} band is due to the ν_3 mode of 1% abundant $^{13}CO_2$ (2284.5 cm^{-1} in gas phase CO_2). The higher frequency bands have been discussed at length by Garrone et al.[44] and attributed by them to combinations of the ν_3 mode with low frequency lattice modes of the zeolite framework. Support for these assignments came from computational results and direct observation of far-infrared bands corresponding to the lattice modes. For CO_2 in Na-Rho, the lattice modes corresponding to the three combination bands observed must have frequencies of 47, 92, and 145 cm^{-1} respectively. These values are different from those reported by Garrone et al. for CO_2 adsorbed in Na-ZSM-5 (two combination bands observed corresponding to lattice mode frequencies of 45 cm^{-1} and 60 cm^{-1}). As discussed by them, however, the low frequency lattice modes vary with the zeolite framework structure and do not depend on the particular cation with which the CO_2 is interacting. The coupling of the ν_3 mode of adsorbed CO_2 with zeolite lattice modes was inferred by Garrone et al. to mean that the primary interaction between oxygen atoms of the adsorbed CO_2 and zeolite cations is accompanied by a secondary interaction between the carbon atoms and adjacent oxide ions of the zeolite lattice.

As the CO_2 coverage is increased in Na-Rho, an additional band appears on the ν_1 region at 1416 cm^{-1}. In light of the structural evidence for two different CO_2 adsorption sites in Na-Rho (see above), we assign this second band to the ν_1 mode of a second form of adsorbed CO_2, occupying sites at higher coverage. As the extinction coefficient for this mode of adsorbed CO_2 will depend strongly on the local symmetry at the adsorption site, it is not possible to quantify from the infrared data the relative amounts of the two species. The occurrence of two different ν_1 frequencies for CO_2 in Na-Rho might be expected to result in different ν_3 frequencies as well, but the intensity and breadth of the ν_3 band at higher coverages prevents confirmation of this.

In the case of Na,Cs-Rho, only the 1378 cm^{-1} band was observed, increasing in intensity with increasing surface coverage (Supporting Information, S12). The infrared measurements thus indicate a single adsorption site for CO_2 in Na,Cs-Rho. The ν_3 region of the spectrum of CO_2 adsorbed in NaCs-Rho is indistinguishable from that in Na-Rho at lower coverages, but any differences would only be evident at higher coverages where bands in this region cannot be resolved. For K-Rho also, a single band was observed in the ν_1 region (Supporting Information, S12), although this band only became evident at pressures higher than those seen with Na-Rho. In the ν_3 region a band at 2351 cm^{-1} was seen for CO_2 in K-Rho at low pressures, although this band was much weaker than those for Na-Rho, NaCs-Rho and Li-Rho at the same pressures. At higher pressures, CO_2 in K-Rho showed higher frequency shoulders and a lower frequency $^{13}CO_2$ component similar to those seen with the other zeolites.

dx.doi.org/10.1021/ja3070864 | J. Am. Chem. Soc. 2012, 134, 17628–17642

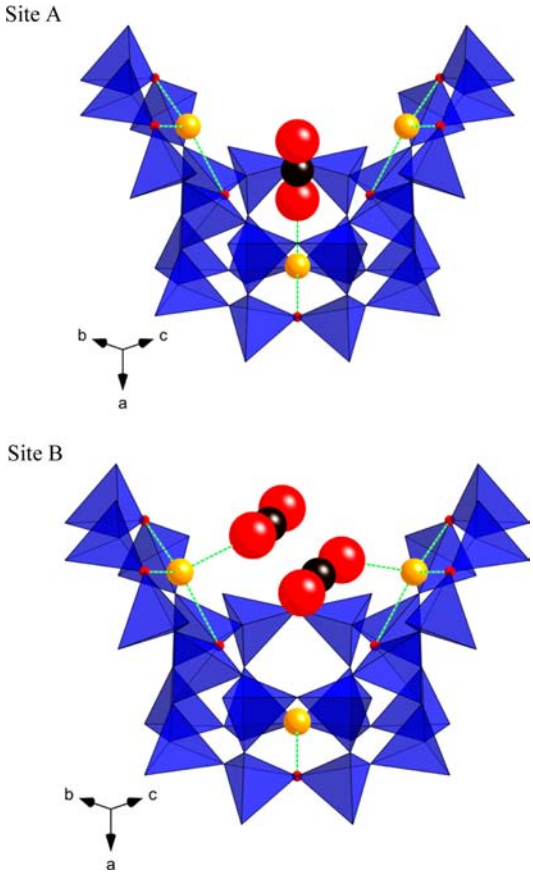

Figure 11. Adsorption sites for CO_2 in Na-Rho, as determined by Rietveld refinement of the synchrotron X-ray diffraction data at 298 K, with an equilibrium pressure of 0.1 bar. In adsorption site A the O═C═O molecules adopt end-on coordination with Na^+ cations (orange spheres) in the S8R site, whereas in site B they directly coordinate a S6R Na^+ cation.

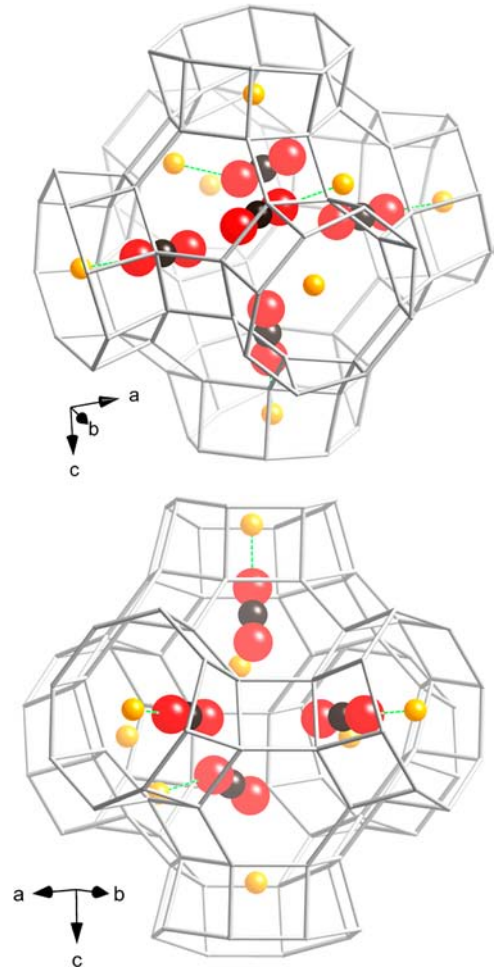

Figure 12. Two possible arrangements of Na^+ cations and CO_2 molecules within an α-cage of Na-Rho that is in equilibrium with 0.1 bar of CO_2 at 298 K. These are based on the refined structure and a consideration of possible arrangements of cations and CO_2 molecules, given the observed statistical occupancies.

In the case of Li-Rho, the ν_1 region shows two distinct bands at all CO_2 coverages (1374 and 1382 cm^{-1}, Supporting Information, S12). Although this might be taken as evidence for the existence of two different CO_2 adsorption sites, an additional band was also seen to appear in parallel at 1635 cm^{-1}, which was not seen with any of the other zeolites. Many authors report bands in this region due to adsorbed carbonate or bicarbonate when CO_2 is adsorbed in alkali metal zeolites, particularly in the presence of adsorbed water. For example, bands at 1670 and 1335 cm^{-1} observed when CO_2 is adsorbed in zeolite KX have been assigned to a bidentate carbonate species[46] (while Galhotra et al.[45] attribute bands at 1640, 1461, and 1381 cm^{-1} to carbonate and bicarbonate species in nanosized NaY zeolites). They further suggest that the presence of adsorbed water enhances the formation of bicarbonate species in BaY. We suggest from these comparisons that small amounts of carbonate and/or bicarbonate species are formed when CO_2 is adsorbed in Li-Rho. In the ν_3 region, CO_2 adsorption in Li-Rho gave initially a band at 2355 cm^{-1}, shifted from the frequency obtained with Na-Rho and Na,Cs-Rho. The higher frequency bands assigned to combination modes are present at approximately the same frequencies as in Na-Rho, Na,Cs-Rho, and K-Rho. Notably, however, the bands due to adsorbed CO_2 in Li-Rho are already well developed at a pressure of 0.25 mbar, more so than with the other zeolites,

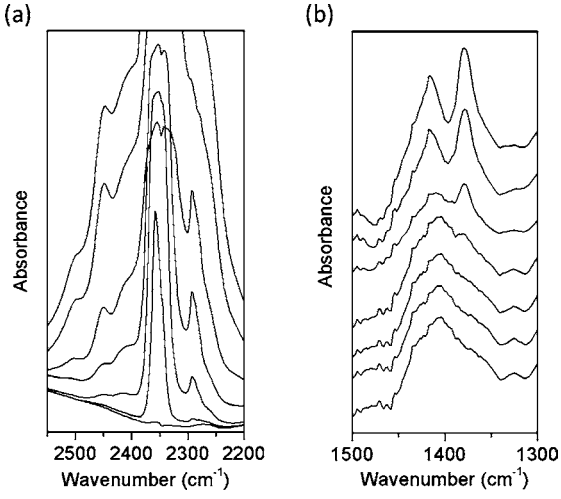

Figure 13. Infrared spectra of CO_2 adsorbed on dehydrated Na-Rho at different equilibrium pressures at room temperature. The increasing signals correspond to CO_2 pressures of 0, 0.25, 5, 10, 25, 50, and 150 mbar.

dx.doi.org/10.1021/ja3070864 | J. Am. Chem. Soc. 2012, 134, 17628−17642

consistent with the different shapes of the adsorption isotherms.

3.3.5. Comparison of Ethane Uptake on Na-Rho with That on Na-ZK-5. The adsorption behavior of ethane on Na-Rho at 298 K was compared with that over H-Rho and Na-ZK-5. Whereas ethane is readily taken up by Na-ZK-5 and H-Rho (at 0.7 bar, the uptakes are 1.8 and 1.65 mmol g^{-1}, respectively), it is effectively blocked from adsorption into Na-Rho (Supporting Information). Ethane is a larger molecule than CO_2 (3.90 Å), so this may be due to the restricted size of the 8MR opening in the presence of cations in the windows or due to the physical presence of the cations; in fact, the two are related. The resultant effect is likely to be high selectivity for Na-Rho for CO_2 over ethane in mixtures, similar to that observed previously for Na,Cs-Rho for CO_2/CH_4 mixtures.[9]

3.3.6. Zero Length Column Analysis of CO_2 Desorption from Na,Cs-Rho and Na-Rho. Dehydrated Na,Cs- and Na-Rho can adsorb CO_2 only if the Na^+ cations move, so that analysis of the desorption data measured by ZLC gives a measure of the rate of the diffusion that relies on this process (See Supporting Information for theoretical details). Figure 14a shows the desorption curves at 308 K for the fully and partially saturated ZLC experiment on the Na,Cs-Rho sample, fitted well by curves assuming a single value for the diffusivity of 0.875×10^{-19} m^2 s^{-1} (calculated using a value of the crystal radius of 50 nm, as measured from the SEM). This diffusivity is calculated from the long-time desorption data, which corresponds to desorption under the Henry's law regime.[47,48]

It was not possible to fit the desorption data for the Na-Rho fully saturated at 10% CO_2 in a similar way (see Supporting Information), but it was possible to fit the desorption curve from a sample of Na-Rho saturated with 1% CO_2 with a single diffusivity, calculated from the long-time desorption data as 1.0×10^{-19} m^2 s^{-1} (Figure 14b), and the same diffusivity value enabled the desorption from the partial saturation experiment to be fitted (Supporting Information). The discrepancy of modeled and observed desorption curve for the fully saturated 10% CO_2 experiment cannot be due mainly to isotherm nonlinearity of the isotherm, since the shape of the desorption isotherm does not differ strongly from that of Cs,Na-Rho. It could be associated with concentration dependence of the diffusivity resulting from the structural changes that occur in Na-Rho with variable CO_2 loading. The conditions for desorption at low coverage will approach those for desorption via diffusion through the empty Na-Rho (*I*-43*m*, α = 14.4137(1) Å, O−O distance = 2.26 Å). As CO_2 is adsorbed into the structure, the distortion of the 8MRs decreases, and it becomes easier for the CO_2 to diffuse at higher coverages.

3.3.7. Summary of the CO_2 Adsorption Mechanism for Na-Rho. For diffusion of CO_2 through the dehydrated Na-form of zeolite Rho, the cations must move away from the sites that they occupy in the windows. The mobility of Na^+ cations via a hopping motion in the presence of CO_2 has previously been predicted for faujasitic Na-X and Na-Y zeolites by molecular dynamics simulations.[49] That the site occupancies in Na-Rho measured by diffraction change little during adsorption and desorption indicates that the cations can rapidly move back to their original site once the CO_2 molecule has passed through the window.

At very low surface coverages on Na-Rho, the diffusivity is estimated from ZLC studies to be 1.0×10^{-19} m^2 s^{-1}. This is significantly lower than the micropore diffusivities for CO_2 on Ca-A (4A) and Ca-X determined by Ahn et al.[50] over the range

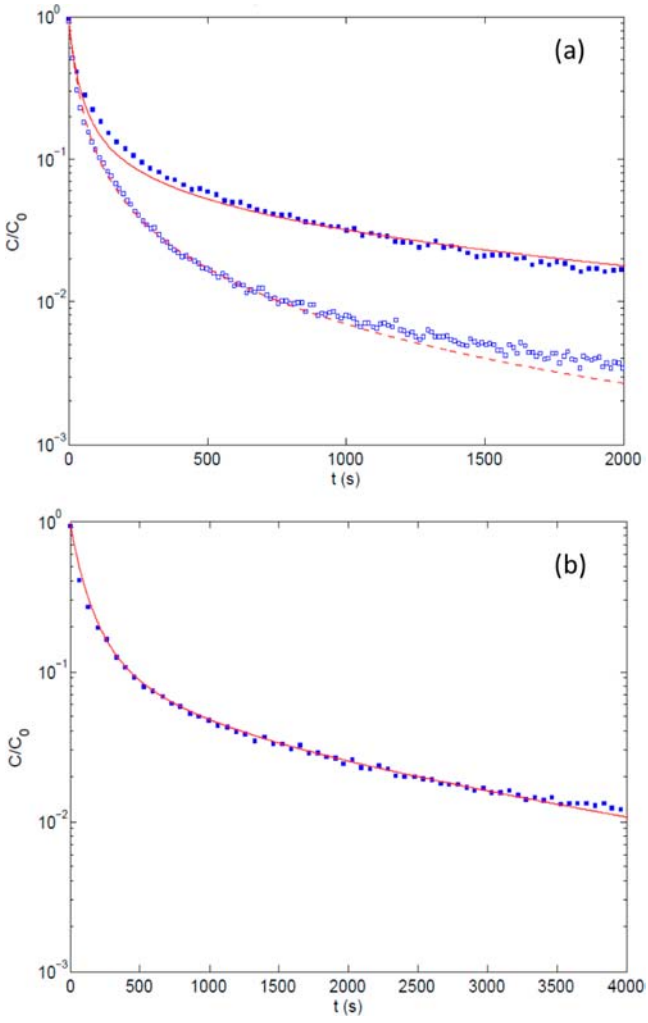

Figure 14. Experimental ZLC desorption curves at 308 K for (a) the fully and partially (5.6 min) saturated Na,Cs-Rho sample using 2 mL/min 10% CO_2 and (b) Na-Rho saturated using 1 mL/min 1% CO_2 and desorbing in a 1 mL/min flow of He. The data are given in blue as individual points (solid for fully saturated, open for partially saturated). The fitted curves (red) are calculated using a single value for the diffusivity as described in eqs 2 and 5 in the Supporting Information.

273−313 K by analysis of gravimetric data to be 10^{-16} and 10^{-14} m^2 s^{-1}, respectively. The diffusivity is increased at higher coverages by the influence of other adsorbed CO_2 molecules and by the increase in 8MR window size (2.75 Å by 0.1 bar, cf. 2.26 Å in the dehydrated form). A suggested mechanism for "trapdoor" CO_2 migration at low coverages is depicted schematically in Figure 15. The presence of additional CO_2 molecules will result in additional coordination of Site II Na^+ cations, reducing the energy for cation displacement, in a similar way to that proposed for the water-mediated migration of Cd^{2+} ions from window sites to S6R sites upon dehydration of Cd-Rho.[51]

4. CONCLUSIONS

Univalent cationic forms of zeolite Rho show remarkable CO_2 adsorption behavior that results from a combination of its flexible framework structure, the distribution of extra-framework cations over different sites, and the mobility of those cations that occupy window sites between α-cages.

dx.doi.org/10.1021/ja3070864 | J. Am. Chem. Soc. 2012, 134, 17628−17642

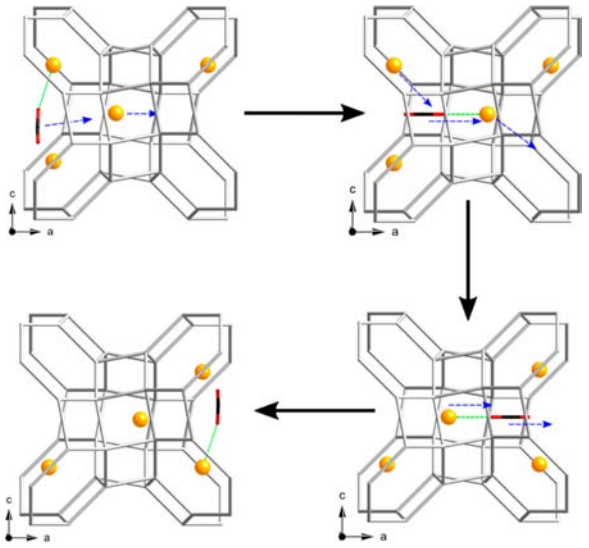

Figure 15. Postulated cooperative mechanism by which CO_2 molecules (represented by red and black sticks) could pass through a window site between α-cages in zeolite Na-Rho, where a Na^+ cation (yellow sphere) occupies one of the S8R sites in the window.

H-Rho has the highest pore volume of all Rho samples examined but does not show strong adsorption of CO_2 at conditions relevant to carbon capture from flue gases. Adsorption is of type I and shows no hysteresis. H-SAPO(RHO) CO_2 interacts more weakly still than the aluminosilicate, due to its lower framework charge. US-Rho, in which there are extra-framework Al species, also takes up less CO_2 at 0.1 bar and 298 K than H-Rho.

The highest values of CO_2 adsorption for zeolite Rho are observed on the lithium form. Li^+ cations are expected to occupy S6R sites in the α-cage and so leave window sites free of cations. As a result the CO_2 adsorption isotherms at 298 K do not show hysteresis. The strong interaction with Li-Rho is expected on electrostatic grounds and also because all the Li^+ cations in the S6R sites are accessible. The ability of Li-Rho to admit CO_2, even though the opening of the windows is only 1.90 Å, indicates that there is sufficient framework flexibility and interaction at 298 K to permit CO_2 diffusion.

In contrast to the Li-Rho behavior, the Na-, K-, NH_4-, and Cs-forms of Rho show hysteresis in their CO_2 adsorption isotherms (Na,NH_4 < K < Cs), with the adsorption at 298 K and 0−1 bar decreasing in the order Na > K, NH_4 > Cs. This effect is much more marked than that expected on the basis of increased cation volume occupying pore space, since Cs-Rho shows very little uptake. In all these cases cations occupy window sites in the dehydrated form, as "sentinels", either in D8R or S8R sites, so there must be cation displacement to allow CO_2 uptake to occur. In Na-Rho the cations occupy S8R sites in the windows, in K- and NH_4-Rho both D8R and S8R sites are occupied, and in Cs-Rho all the D8R sites are occupied. The movement of larger cations to S8R sites (as previously observed to occur for Cs^+ cations at pressures greater than 1 bar in Na,Cs-Rho) results in a decrease in the coordination of the cation by framework oxygen atoms and a distortion away from *I*-43*m* to *Im*-3*m* which involves an energetic cost.

No such hysteresis in CO_2 adsorption isotherms is observed for the Na-form of ZK-5, which does not have cations in positions that block windows between the α-cages. The uptakes on the Na- (and also the Li-) forms of ZK-5 are high at low CO_2 pressures, but the selectivity to CO_2 over other gases (e.g., light hydrocarbons) is much lower because there is no barrier to their adsorption. The unprecedented selectivity of Na,Cs-Rho to CO_2 over CH_4 reported by Palomino et al.[9] and the high ratio of single component adsorption uptakes of CO_2 to ethane over Na-Rho reported here results from the ability of sodium cations to move to allow the passage of CO_2 molecules into Rho while the larger size (4 Å) and lower interaction of hydrocarbons results in their exclusion.

The Na^+ cations in fully exchanged Na-Rho remain in S8R and S6R positions during adsorption and CO_2 molecules occupy two positions, in each of which the O═C═O molecule adopts end-on coordination with one Na^+ cation and may interact with another. The stronger of these adsorption sites involves one cation in a S8R site; the other involves interaction with a Na^+ cation in a S6R site. Upon desorption of CO_2 from Na-Rho at 298 K, there is a gradual decrease in the single unit cell *a* parameter within the *I*-43*m* space group, indicating a concerted structural change, and ZLC measurements of desorption indicate a "zero-coverage" diffusivity of 1.0×10^{-19} m^2 s^{-1} at 308 K. At these low loadings there is reduced window size, and fewer CO_2 molecules able to act to mediate the displacement of cations away from window sites where they block molecular transport. The transport is faster at higher loadings.

Fully exchanged Na-Rho is the most promising CO_2 adsorbent of those studied, when taking into account cost, uptake, selectivity, and kinetics. Adsorption occurs on S8R and S6R sites: that these two adsorption sites exist is a consequence of both framework and extra framework composition, so that manipulation of these can give rise to "adsorption site engineering". It should therefore be possible to modify chemical composition to optimize CO_2 uptake with this knowledge of the structural chemistry of Rho.

That Na-Rho (and the NH_4^+ and K^+ forms) demonstrate reversible uptake of CO_2 at all is due to the ability of the cations in window sites to undergo local displacement, leading to a proposed mechanism that involves a CO_2-mediated migration from a window site to a vacant α-cage site. The selectivity for CO_2 over small hydrocarbons observed over Na-Rho arises from the difficulty for small hydrocarbons (diameter 4 Å) to pass through windows that are both highly elliptical and also blocked with cations. Future studies will aim to deconvolute the roles of cation−adsorbate interactions and molecular sieving in determining this selectivity.

Na-Rho could be used as a selective CO_2 adsorbent in kinetic gas separation applications, either as a packed bed or in membrane form. The extended time to achieve full desorption of adsorbed CO_2 observed by measurement of adsorption isotherms and by ZLC suggest temperature swing adsorption may be more appropriate than pressure swing adsorption applications. Furthermore, it should be possible to optimize its uptake and diffusional properties by modification of framework and mixed cation composition. It is also likely that the trapdoor behavior and high selectivity of zeolite Rho will be observed in structurally related and similarly flexible zeolites, widening the types of observed adsorption behavior in zeolitic solids.

■ ASSOCIATED CONTENT

Ⓢ Supporting Information

Details of the syntheses, powder diffraction patterns, ion exchange conditions, TGA data, structural and refinement

dx.doi.org/10.1021/ja3070864 | J. Am. Chem. Soc. 2012, 134, 17628−17642

details as well as crystallographic information files, additional adsorption isotherm data, solid state NMR and full infrared spectra. This material is available free of charge via the Internet at http://pubs.acs.org.

AUTHOR INFORMATION

Corresponding Author

paw2@st-andrews.ac.uk

Notes

The authors declare no competing financial interest.

ACKNOWLEDGMENTS

We gratefully acknowledge the EPSRC (EP/G062129/1, Innovative Gas Separations for Carbon Capture: M.M.L., E.M., S.B., P.A.W.) for funding, Mrs. Sylvia Williamson for collection of the adsorption isotherms, Professor Chiu C. Tang for assistance at the I-11 beamline at the Diamond Light Source (DLS), and DLS for beamtime. Solid State NMR spectra were obtained at the EPSRC facility in Durham. Drs. Miguel Palomino and Susanna Valencia and Professors Fernando Rey and Avelino Corma are thanked for helpful discussions.

REFERENCES

(1) Barrer, R. M.; Gibbons, R. M *Trans. Faraday Soc.* **1965**, *61*, 948−961.

(2) Pirngruber, G. D.; Raybaud, P.; Belmabkhout, Y.; Cejka, J.; Zukal, A. *Phys. Chem. Chem. Phys.* **2010**, *12*, 13534−13546.

(3) Palomino, M.; Corma, A.; Rey, F.; Valencia, S. *Langmuir* **2010**, *26*, 1910−1917.

(4) Ridha, F. N.; Yang, Y. X.; Webley, P. A. *Microporous Mesoporous Mater.* **2009**, *117*, 497−507.

(5) Ridha, F. N.; Webley, P. A. *Sep. Purif. Technol.* **2009**, *67*, 336−343.

(6) Ridha, F. N.; Webley, P. A. *Microporous Mesoporous Mater.* **2010**, *132*, 22−30.

(7) Hudson, M. R.; Queen, W. L.; Mason, J. A.; Fickel, D. W.; Lobo, R. F.; Brown, C. M. *J. Am. Chem. Soc.* **2012**, *134*, 1970−1973.

(8) Robson, H. E.; Shoemaker, D. P.; Ogilvie, R. A.; Manor, P. C. In *Molecular Sieves*; Meier, W. M., Uytterhoeven, J. B., Eds.; American Chemical Society: Washington, DC, 1973; *Adv. Chem. Ser. No.* 121, p 106.

(9) Palomino, M.; Corma, A.; Jorda, J. L.; Rey, F.; Valencia, S. *Chem. Commun.* **2012**, *48*, 215−217.

(10) Parise, J. B.; Abrams, L.; Gier, T. E.; Corbin, D. R.; Jorgensen, J. D.; Prince, E. *J. Phys. Chem.* **1984**, *88*, 2303−2307.

(11) Araki, S.; Kiyohara, Y.; Tanaka, S.; Miyake, Y. *Chem. Lett.* **2012**, *41*, 125−126.

(12) Parise, J. B.; Abrams, L.; Gier, T. E.; Corbin, D. R.; Jorgensen, J. D.; Prince, E. *J. Phys. Chem.* **1984**, *88*, 203.

(13) Corbin, D. R.; Abrams, L.; Jones, G. A.; Eddy, M. M.; Harrison, W. T. A.; Stucky, G. D.; Cox, D. E. *J. Am. Chem. Soc.* **1990**, *112*, 4821−4830.

(14) Fischer, R. X.; Baur, W. H.; Shannon, R. D.; Staley, R. H.; Vega, A. J.; Abrams, L.; Prince, E. *J. Phys. Chem.* **1986**, *90*, 4414−4423.

(15) (a) Johnson, G. M.; Reisner, B. A.; Tripathi, A.; Corbin, D. R.; Toby, B. H.; Parise, J. B. *Chem. Mater.* **1999**, *11*, 2780−2787. (b) Corbin, D. R. U.S. Patent 7,169,212, 2007

(16) Eic, M.; Ruthven, D. M. *Zeolites* **1988**, *8*, 472−479.

(17) Ruthven, D. M.; Brandani, S.; Eic, M. *Mol. Sieves* **2008**, *7*, 45−84.

(18) Brandani, S.; Hufton, J.; Ruthven, D. M. *Zeolites* **1995**, *15*, 624−631.

(19) Brandani, S.; Ruthven, D. M. *Adsorption* **1996**, *2*, 133−143.

(20) Lievens, J. L.; Verduijn, J. P.; Mortier, W. J. *Zeolites* **1992**, *12*, 690−697.

(21) Verduijn, J. P. U.S. Patent 5,944,249, 1991.

(22) Pulido, A.; Nachtigall, P.; Zukal, A.; Dominguez, I.; Cejka, J. *J. Phys. Chem. C* **2009**, *113*, 2928−2935.

(23) Zukal, A.; Arean, C. O.; Delgado, M. R.; Nachtigall, P.; Pulido, A.; Mayerova, J.; Cejka, J. *Microporous Mesoporous Mater.* **2011**, *146*, 97−105.

(24) Chatelain, T.; Patarin, J.; Fousson, E.; Soulard, M.; Guth, J. L.; Schulz, P. *Microporous Mater.* **1995**, *4*, 231−238.

(25) Araki, S.; Kiyohara, Y.; Tanaka, S.; Miyake, Y. *J. Colloid Interface Sci.* **2012**, *376*, 28−33.

(26) Su, X.; Tian, P.; Li, J.; Zhang, Y.; Meng, S.; He, Y.; Fan, D.; Liu, Z. *Microporous Mesoporous Mater.* **2011**, *144*, 113−119.

(27) Langmi, H. W.; Book, D.; Walton, A.; Johnson, S. R.; Al-Mamouri, M. M.; Speight, J. D.; Edwards, P. P.; Harris, I. R.; Anderson, P. A. *J. Alloys Compd.* **2005**, *404*, 637−642.

(28) Udovic, T. J.; Cavanagh, R. R.; Rush, J. J.; Wax, M. J.; Stucky, G. D.; Jones, G. A.; Corbin, D. R. *J. Phys. Chem.* **1987**, *91*, 5968−5973.

(29) Fischer, R. X.; Baur, W. H.; Shannon, R. D.; Staley, R. H. *J. Phys. Chem.* **1987**, *91*, 2227−2230.

(30) Fischer, R. X.; Baur, W. H.; Shannon, R. D.; Staley, R. H.; Abrams, L.; Vega, A. J.; Jorgensen, J. D. *Acta Crystallogr.* **1988**, *B44*, 321−334.

(31) Larson, A. C.; Von Dreele, R. B. *General Structure Analysis System (GSAS)*; Los Alamos National Laboratory: Los Alamos, 1994.

(32) Cartlidge, S.; Meier, W. M. *Zeolites* **1984**, *4*, 218−225.

(33) Thompson, S. P.; Parker, J. E.; Potter, J.; Hill, T. P.; Birt, A.; Cobb, T. M.; Yuan, F.; Tang, C. C. *Rev. Sci. Instrum.* **2009**, *80*, 075107−9.

(34) Parker, J. E.; Potter, J.; Thompson, S. P.; Lennie, A. R.; Tang, C. C. *Mater. Sci. Forum* **2012**, *706−709*, 1707−1712.

(35) Yu, Z. W.; Zheng, A. M.; Wang, Q. A.; Chen, L.; Xu, J.; Amoureux, J. P.; Deng, F. *Angew. Chem., Int. Ed.* **2010**, *49*, 8657−8661.

(36) Cook, M.; Conner, W. C. in *Proceedings of the 12th International Zeological Conference*; Treacy, M. M. J., Marcus, B. K., Bisher, M. E., Higgins, J. B., Eds.; Materials Research Society, Warrendale, PA, 1999; p 409.

(37) Vrabec, J.; Stoll, J.; Hasse, H. *J. Phys. Chem. B.* **2001**, *105*, 12126−12133.

(38) Fischer, R. X.; Baur, W. H.; Shannon, R. D.; Parise, J. B.; Faber, J.; Prince, E. *Acta Crystallogr.* **1989**, *C45*, 983−989.

(39) Tian, P.; Su, X.; Wang, Y.; Xia, Q; Zhang, Q.; Fan, D.; Meng, S.; Liu, Z. *Chem. Mater.* **2011**, *23*, 1406−1413.

(40) Cheung, O.; Liu, Q. L.; Bacsik, Z.; Hedin, N. *Microporous Mesoporous Mater.* **2012**, *156*, 90−96.

(41) McCusker, L. B. *Zeolites* **1984**, *4*, 51−55.

(42) Liu, Q.; Pham, T.; Porosoff, M. D.; Lobo, R. F. *ChemSusChem* **2012**, DOI: 10.1002/cssc.201200339.

(43) (a) Bourrelly, S.; Llewellyn, P. L.; Serre, C.; Millange, F.; Loiseau, T.; Férey, G. *J. Am. Chem. Soc.* **2005**, *127*, 13519−13521. (b) Llewellyn, P. L.; Bourrelly, S.; Serre, C.; Filinchuk, Y.; Férey, G. *Angew. Chem., Int. Ed.* **2006**, *45*, 7751−7754. (c) Coudert, F. X.; Boutin, A.; Jeffroy, M.; Mellot-Draznieks, C.; Fuchs, A. H. *ChemPhysChem* **2011**, *12*, 247−258.

(44) Garrone, E.; Bonelli, B.; Lamberti, C.; Civalleri, B.; Rocchia, M.; Roy, P.; Otero-Arean, C. *J. Chem. Phys.* **2002**, *117*, 10274−10282.

(45) Galhotra, P.; Navea, J. G.; Larsen, S. C.; Grassian, V. H. *Energy Environ. Sci.* **2009**, *2*, 401−409.

(46) Siporin, S. E.; McClaine, B. C.; Davis, R. J. *Langmuir* **2003**, *19*, 4707−4713.

(47) Brandani, S. *Chem. Eng. Sci.* **1998**, *53*, 2791−2798.

(48) Brandani, S.; Jama, M. A.; Ruthven, D. M. *Chem. Eng. Sci.* **2000**, *55*, 1205−1212.

(49) Plant, D. F.; Maurin, G.; Jobic, H.; Llewellyn, P. L. *J. Phys. Chem. B* **2006**, *110*, 14372−14378.

(50) Ahn, H.; Moon, J.-H.; Hyun, S.-H.; Lee, C.-H. *Adsorption* **2004**, *10*, 111−128.

(51) Reisner, B. A.; Lee, Y.; Hanson, J. C.; Jones, G. A.; Parise, J. B.; Corbin, D. R.; Toby, B. H.; Freitag, A.; Larese, J. Z.; Kahlenberg, V. *Chem. Commun.* **2000**, 2221−2222.